Study of Gas Mobility Control during CO_2 Injection for Enhanced Oil Recovery

Master Thesis in Reservoir Physics

Tor Aksel Lystad

Department of Physics and Technology

University of Bergen

June 2016

Abstract

Carbon Dioxide (CO_2) has been used as a commercial source for Enhanced Oil Recovery (EOR) for over 40 years. In recent years, the utilization of anthropogenic CO_2 has become more attractive, because of its proven EOR and climate mitigating capability. Despite the EOR potential, it is widely known that many CO_2 injection projects are associated with inefficient gas utilization, poor macroscopic sweep efficiencies and low recoveries caused by effects of gravity segregation and viscous instabilities. Effective and affordable optimization of CO_2 mobility has the potential to prolong the lifetime of existing hydrocarbon reservoirs and recover additional oil with carbon-neutral EOR activity.

This thesis is part of an international collaboration, including 10 oil and service companies and 13 universities and research institutions in both USA and Europe, initiated to gain experience and confidence in utilizing CO_2 for EOR. The aim for the research program is to perform laboratory studies combined with up-scaling techniques, through numerical simulation, and ultimately conduct field pilots at four confirmed onshore locations in Texas and Mississippi, United States.

The experimental work conducted in this thesis investigates the use of mobility control with foam during CO_2-EOR in strongly water-wet Edwards Limestone core plug samples of heterogeneous porosity and permeability. Tertiary co-injection of supercritical state CO_2 and a surfactant to generate foam was conducted after a waterflood to resemble EOR projects in mature hydrocarbon reservoirs. The tertiary displacements were conducted as either CO_2-foam (three experiments) or as a baseline test (one experiment) without foaming agent present. The baseline test was performed to evaluate the importance of generating foam in terms of mobility control. All co-injections were conducted at fixed liquid and gas fractions, with a total injection rate of 10 ml/h. On four stacked core systems, total oil recoveries ranged from 69.3% to 87.0% of Original Oil in Place (OOIP), with the baseline test being the most effective. Results show that additional oil recovered during the co-injections were dependent on foam stability, liquid-gas fractions and overall connectivity in the heterogeneous medium.

Using Eclipse reservoir simulator, a history matching of the experimental results was performed. The simulation base model was built by collecting observed experimental liquid production data and combined with the measured core properties of core system used in the baseline test. The aim was to obtain satisfactory history match between simulated and laboratory data by conducting sensitivity parameter studies. A validated numerical model, i.e. a model that reproduce the experimental results observed, may be used for up-scaling from the laboratory scale towards the field pilot scale. It was observed that the concurrence of simulated and laboratory waterflood data was dependent on crude oil and brine relative permeabilities.

Acknowledgements

I would like to express my gratitude to Professor Arne Graue and the reservoir physics research group at the Department of Physics and Technology at University of Bergen for giving me the opportunity and resources to work on something as interesting and challenging as this thesis proved out to be. Thanks to my supervisor, Associate Professor Martin Fernø, for the guidance and for contributing with your knowledge and experience in relevant discussions.

Thank you to PhD candidates Sunniva Brudvik Fredriksen for the knowledge and patience you showed while working with me and thank you for assembling a great research-team. Thanks to PhD candidate Zachary Paul Alcorn for the contribution and collaboration in the laboratory work and the guidance during numerical simulation. I wish both of you the best of luck finishing your Doctorate's Degree.

Cheers to all my fellow graduates. The last few months finishing this thesis have been chaotic, but all of you contributed to a fun and mellow atmosphere. I would also like to shout out Josef Flatlandsmo, Lars Korbøl Nordtveit and Erik Rasmussen Vadla for all the fun we have had over the last five years.

I would also like to thank my good friend and roommate Kristoffer Dahl Sagmo for being the kind and laidback guy that you are. We have come a long way since we first moved to Bergen from Trondheim.

Thanks to my family, Jan Erik Lystad, Gunn Hagen Lystad, Vegard Lystad and Håkon Lystad. I appreciate the support you guys have showed on all levels throughout my education. Mama, I made it.

Finally, I would like to thank Pia Lucie Skaanes. Thank you for being understanding and supportive. I know that your patience is exhausted, but this very moment is what we have been waiting for.

Bergen 01.06.2016

Tor Aksel Lystad

Table of Contents

Abstract **1**

Acknowledgements **2**

Table of Contents **3**

Preface **5**

Carbon Capture Utilization and Storage (CCUS) 7

Field Pilot Research Program 8

Reservoir Scaling Technique 8

1. Oil Recovery in Carbonate Reservoirs **9**

1.1 Production Mechanisms 9

1.2 Carbonate Reservoirs 10

1.2.1 Heterogeneity 10

1.2.2 Fractured Reservoirs 10

1.2.3 Pore Size Distribution 11

2. CO_2 Enhanced Oil Recovery and Mobility Control with Foam **12**

2.1 Properties of CO_2 and Surface Active Agents 12

2.2 CO_2-Foam 13

2.2.1 Foam Generation 14

2.2.2 Foam Quality 15

2.2.3 Foam Stability 16

2.3 Mobility Control with CO_2-Foam 17

3. Experimental Setup and Procedure **19**

3.1 Volumetric Change Parameter 19

3.2 Rock Material and Fluids 20

3.3 Routine Core Analysis 21

3.3.1 Porosity 21

3.3.2 Absolute Permeability 22

3.3.3 Core Assembly and System Pressurization 23

3.4 Mobility Control 24

3.4.1 Experimental Setup 24

3.4.2 Apparatus 25

3.4.3 Primary Drainage 25

3.4.4 Waterflooding 26

3.4.5 Co-injection 27

3.5 Numerical Simulation 28

4. Results and Discussion 29
4.1 Routine Core Analysis 29
4.2 Results Overview 31
4.2.1 Primary Drainage 31
4.2.2 Waterflood 32
4.3 Mobility Control 33
4.3.1 Foam Stability 35
4.3.2 Oil Recovery by Mobility Control 36
4.3.3 Oil Recovery by CO_2 Dissolution 37
4.3.4 Oil Recovery by Vertical Injection 37
4.3.5 Baseline Test 38
4.4 Numerical Simulation 40
4.4.1 Simulated Waterflood 40
4.4.2 Simulated Co-injection 43
5. Concluding Remarks 44
5.1 Conclusions 44
5.2 Future Work 45
Appendix I – Abbreviations and Nomenclature 46
Appendix II – Fundamental Parameters 47
Wettability 47
Absolute, Effective and Relative Permeability 48
Interfacial Tension 49
Capillary Pressure 49
Mobility 50
Miscibility 51
First-contact 52
Multiple-contact 52
Minimum Miscibility Pressure 52
Appendix III – Uncertainties 53
Calculating uncertainties 53
Instrumental Uncertainties 53
Sources of Error 54
Appendix IV – References 55
Appendix V – Simulation Data File 59

Preface

The petroleum industry faces an important and very critical question in this period in time; how to produce oil and gas in today's market, meeting energy demands that are environmentally and economically sustainable? The answer is complex and most likely impossible for one man to answer. This has to be dealt with in a joint effort with contributions from not only the petroleum industry itself, but also governments and institutions of academia all around the world. The increased emission of greenhouse gases is becoming one of the major issues to consider in order to sustain a healthy living environment. Two key paragraphs were written in the Fifth Assessment Report issued by the Intergovernmental Panel on Climate Change (IPCC) in 2014 stating: *"Human influence on the climate change is clear, and recent anthropogenic emissions of greenhouse gases are the highest in history… The atmosphere and ocean have warmed, the amounts of snow and ice have diminished, and sea level has risen."* (IPCC, 2014). Anthropogenic greenhouse gas emission is mainly driven by local climate policies, economy, energy usage, technology, population size and lifestyle. *"Continued emission of greenhouse gases will cause further warming and long-lasting changes in all components of the climate system, increasing the likelihood of severe, pervasive and irreversible impacts for people and ecosystems."* (IPCC, 2014). Climate change is linked to the use of energy and the emission of greenhouse gases, where CO_2 is the most prominent of the gases. Figure 1.1 shows a pie chart of shares of global CO_2 gas emission and yearly CO_2 gas emission from fossil fuel combustion.

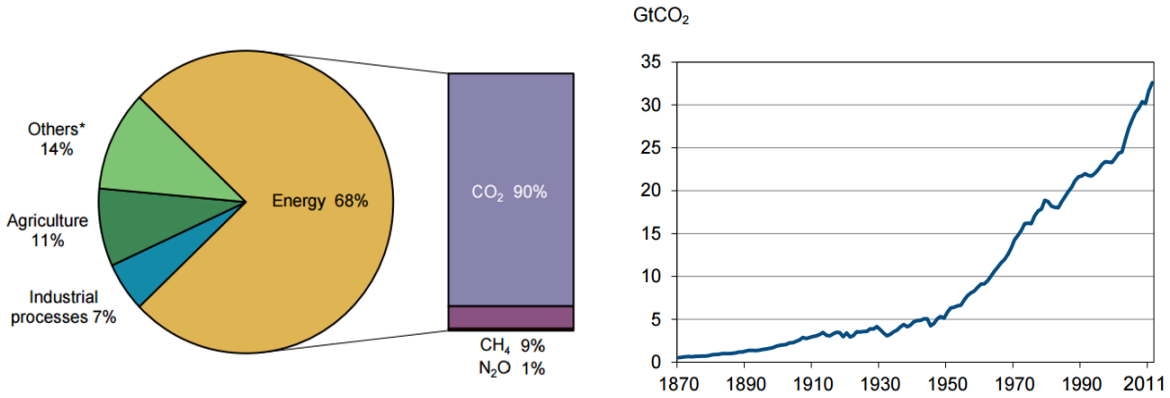

Figure 1.1: Left: Pie chart illustrating the shares of global anthropogenic greenhouse gas emission. CO_2 is the major contributor, accounting for 90% of greenhouse gas emission within the energy sector. (IEA, 2015). Right: CO_2 emission from fossil fuel combustion dated back to the end of the Industrial Revolution. (IEA, 2015).

Large amounts of CO_2 emitted yearly originate from combustion of fossil fuel, which again originate from oil and gas reservoirs. Fossil fuel is consumed everywhere across the globe, ranging from cars, to houses, to big power plants delivering electricity and remote district heating. Figure 1.2 illustrates the CO_2-emission by sector. Heat and electricity are globally the heaviest contributors to CO_2 gas emission, which in 2013 accounted for 42% of the global share of CO_2 emission. The second largest contributor is the transportation sector (23%). According to the U.S. Federal Highway Administration, 189 million automobile ownership were registered in 1990. In 2007, the number was 247 million. China on the other hand had 16 million automobile ownership registered in 2000 and in 2014, after a staggering growth, this number had increased to 154 million. Although, some of these cars are hybrids or electric, which gives them little or no CO_2-footprint (not including the emission that originates from construction, recharging and destruction), the majority are fossil fueled, making the transportation

sector a contributor to growth in greenhouse gas emission. Industry, tertiary services and other residential energy consumption accounts for 28% of global CO_2 emission. The remaining 7% includes fishing, agriculture and other CO_2-gas emission not specified by any of the other sectors (IEA, 2015).

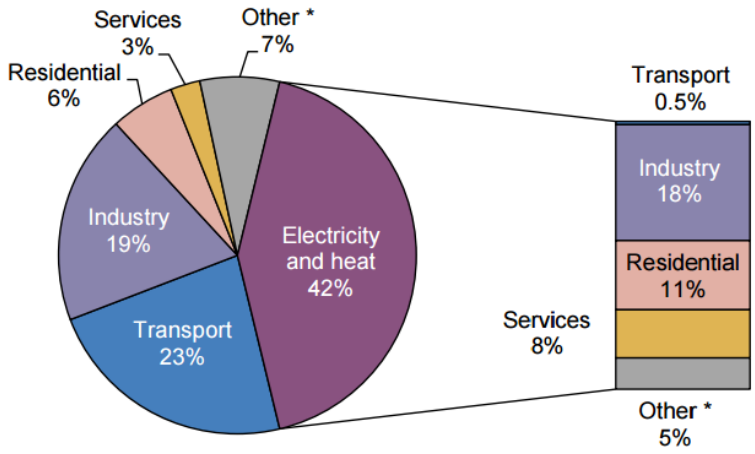

Figure 1.2: Pie chart of global CO_2 emission by sector in 2013. Note that electricity, heat and transport account for nearly two thirds of all CO_2 emitted globally. (IEA, 2015)

The exponential growth of CO_2-emission is closely correlated to the introduction and use of fossil fuel. The industrial revolution marks a turning point in human history as new machine tools improved the manufacturing efficiency in industries such as textile, power and iron. It also marks an important point in the history of anthropogenic emission. The industrial revolution gave a new way to approach mass production through factories and the emission of greenhouse gases has increased ever since. Figure 1.3 graphically illustrates the increase in anthropogenic CO_2 emissions since the industrial revolution.

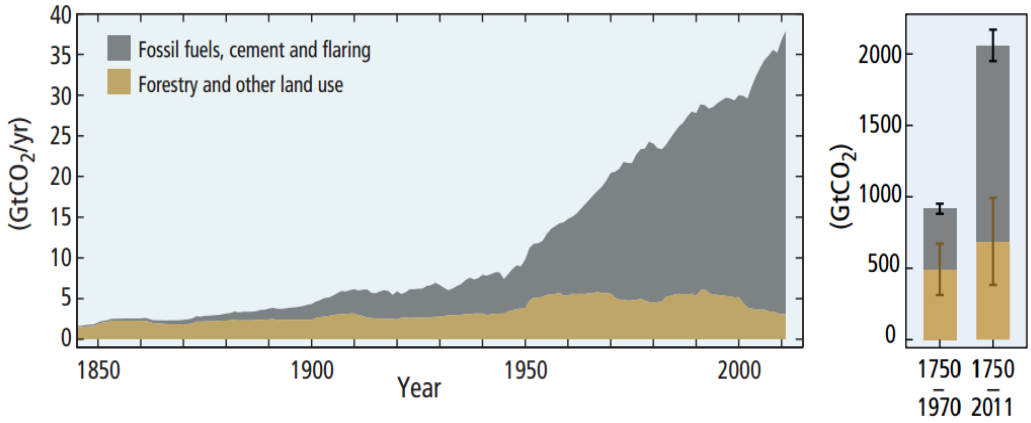

Figure 1.3: Left: illustration of global anthropogenic CO_2 emission per year broken down into two categories, fossil fuels and forestry or other land use. Right: Cumulative CO_2 emissions. Note that the cumulative volume of CO_2 emitted between 1750 and 1970 has tripled between 1970 and 2011 (IPCC, 2014).

The world as we know it today is not environmentally sustainable, which leads to question what to do next. One option could be to completely conclude all oil and gas activity and pursue with renewable sources such as wind, solar and hydroelectric power. Due to the expected population growth and energy demands over the next thirty years, a quick transition to renewables is not a viable option. Fossil fuels, especially natural gas from unconventional sources, will play an increasing and crucial role in the energy mix in 2050 (WEC, 2013). The worldwide energy demand will increase and the only we know for sure is that energy sources in the future have to be affordable, available, reliable and clean.

Carbon Capture Utilization and Storage (CCUS)

One way to meet our future energy demands is to implement a cleaner use of current energy sources. The increased emission of CO_2 gas has led to research and investigation on whether or not it can be used to increase oil recovery through CCUS. Utilization of captured CO_2 at existing or new power plants for integrated EOR or storage can mitigate global climate change while meeting higher demands for energy. The need for increased energy production and the reduction of anthropogenic CO_2 emission may seem contradictory, but the solution might be to utilize anthropogenic CO_2 captured at stationary sources for either integrated EOR at mature waterflooded petroleum reservoirs with residual reserves, or storage in depleted petroleum reservoirs or aquifers. This section of the thesis will discuss the general idea behind CCUS, whereas the focus of the thesis is centered on CO_2-EOR.

The first use of CO_2-EOR dates back to 1972 at the SACROC unit in Texas and to this day, the U.S. are still one of the front-running countries for such oil recovery technology with over 100 ongoing CO_2 projects (Lambert et al., 1996, Sundset, 2011). Despite the potential for CO_2-EOR or storage with the use of CCUS and the number of usable, mature, waterflooded reservoirs, the implementation of this technology has been slow. The apparent cost of CO_2, the infrastructural cost, lack of incentives and general concerns about the effectiveness, proves to be key arguments that delay the development. In addition to cost, there are infrastructural challenges related to CCUS. Fields and sites located in close proximity to a power plant have an advantage when it comes to transport of the gas if the power plant is equipped with the necessary installment needed to separate CO_2 from the bi-product. In the Permian Basin, a network of 5000 kilometers CO_2-pipelines are already installed, covering important states such as Texas, New Mexico, Colorado and Mississippi (Sundset, 2011, Wallace and Kuuskraa, 2014). The Norwegian Continental Shelf (NCS) on the other hand is a much more expensive and difficult site to implement CO_2-EOR with CCUS. Not only because it is located offshore outside the Norwegian coast, but also because the CO_2 would have to be transported in pipelines at locations where temperatures makes it vulnerable to formation of pipeline hydrates (Light component gases such as methane, ethane, nitrogen and CO_2 bound in cavities within solid structures of water) (Sloan and Koh, 2008).

Cost is effectively the prominent issue related to development and implementation of CCUS. The carbon capture part alone is a large investment to make and it is essentially based on incentives by tax deduction and subsidies given by governments around the world. Different governments have different interests and because of this, the cost of such development vary, in fact up to several hundred percent depending on country, state, company and if it is a new or existing construction (Sundset, 2011). As of today, there are 15 operational storage projects and 4 being developed for 2016, including Quest in North America, which is the first large-scale CCUS project to exclusively store CO_2 in a deep marine saline formation and the first since Snøhvit became operational in Norway in 2008 (GCCSI, 2015). For CCUS to work, it would have to be approved and recognized as a viable solution for climate change mitigation. Incentives and subsidiaries given by governments towards EOR or storage are important to increase the number of large-scale projects being developed. To meet climate targets set for 2040, an estimation of 4000 million tonnes of CO_2 per year would have to be captured and stored. This number overshadows the current number of CCUS projects that are either planned, developing or operational, which accounts for a capture capacity of approximately 80 million tonnes of CO_2 per year (GCCSI, 2015). Future energy demands, environmental concerns and advance in technology align to generate opportunities governments, companies and other parties should be inclined to utilize.

Field Pilot Research Program

To gain experience and confidence in CO_2-EOR it is important to bring the laboratory work to the field for testing. An international collaboration, including 10 oil and service companies and 13 universities and research institutions in both USA and Europe, is therefore initiated where the primary objective is to advance technology of CO_2 integrated EOR and aquifer storage. The collaboration allocates tasks, each led by key personnel at their respective institution. The aim is to scientifically perform seven main tasks and combine knowledge and experience gained at the laboratory for further testing at four confirmed onshore U.S. field pilots, in both carbonate and sandstone reservoirs. The Reservoir Physics group, led by Professor Arne Graue at the Department of Physics and Technology at University of Bergen, are contributing with laboratory up-scaling and visualization of EOR with the use of foam. This thesis will therefore revolve around the subject of optimizing mobility of injected CO_2 by using CO_2-foam and then reproduce and visualize the results via numerical simulation using Eclipse and Petrel.

Two of the field pilots are held at East Seminole (carbonate) and Ft. Stockton (sandstone) fields in west Texas, U.S. and if the field pilots are proven successful, the technology can be introduced and applied to fields on the Norwegian Continental Shelf (NCS). Several of the larger fields on the NCS are mature sandstone and carbonates, which have been waterflooded for many years, making them a prime target for CO_2-EOR implementation and a significant storage capacity. Water injection has been the main production method in Norway and as of 2015, the remaining reserves were 2,8 billion Sm^3 (1 billion Sm^3 Oil, 1,8 billion Sm^3 Gas, not including NGL and Condensate) (NPD, 2015).

Reservoir Scaling Technique

Reservoir up-scaling is a technique where experiments performed on laboratory scales are up-scaled in size to evaluate fluid flow behavior, without changing the fundamental structure of the investigation. Recovery and production behavior studied in laboratory experiments are performed on scales that differ from the size of an actual petroleum reservoir. Miscible displacement performed on a core scale has the capability to produce all Oil in Place (OIP) and the complexity of this hydrocarbon displacement is evident and expected outcomes might differ when performed on a larger scale. Because of this disparity, drawing conclusions on performance, production or behavior of the reservoir must be executed carefully. The scaling technique is very much an individual field of study as well as a tool for reservoir engineers looking to implement laboratory work on the reservoir or field scale.

This thesis focuses on displacement mechanisms present at the core scale. All laboratory experiments are conducted on 2'' diameter Edwards Limestone core plugs, with varying length. Mechanisms at play during a laboratory experiment include interactions between fluid and rock, fluid flow and chemical and thermodynamic processes. A reproduction of the experiments are conducted in the Eclipse Simulation Launcher and Petrel to establish a correlation between observed laboratory production data and simulated data. A successful correlation provides a base model that resembles the core properties that is used to perform sensitivity studies. The method enables the up-scaling and interpretation of oil displacement mechanisms on scales that are several orders of magnitude larger.

1. Oil Recovery in Carbonate Reservoirs

In this chapter of the thesis, several petroleum industry terms and other fundamental parameters will be discussed. These will be highlighted in *italic* and if not described, they are found in Appendix II.

1.1 Production Mechanisms

Conventional Production is a term used in the industry for describing production methods that deplete hydrocarbons with the use of natural drive mechanisms present in an environment where oil and gas are found. Hydrocarbons can be found in deposits buried deep underneath the surface of the Earth in a variety of rock formations (e.g. sandstone, carbonates, chalk and shale). Temperatures and pressures are high and required for generation of oil and gas. High pressure and temperature also favorably affects the physical properties of fluids and makes it possible to produce oil and gas from the reservoir. The production of oil and gas are dependent on several forces present in a reservoir, such as compaction pressure caused by millions of years of burial, the natural force applied by expansion of gas, buoyancy effects from surrounding water and gravity. Conventional production mainly covers two categories of oil recovery, known as Primary Recovery and Secondary Recovery.

Primary recovery covers three production mechanisms. 1) Water Drive occurs if the reservoir is connected with a near-proximity source of water, called an aquifer. If the pressure in the aquifer is sufficient, it may be able to drive the oil out of the reservoir. 2) Gas Cap Drive occurs if a gas-phase is present on top of the oil-phase. As the oil flow towards the production well, the gas cap expands supplementing the necessary pressure to drive the oil out of the reservoir. 3) Solution Gas Drive occurs in reservoirs where there are lighter hydrocarbon components present in the oil phase. As oil is produced, the pressure in the reservoir is reduced, allowing the lightest components to liberate out of the oil-zone as gas bubbles. These bubbles will rise to either mix in to or create a gas cap above the oil-zone, where gas expansion will support the production of oil. Although sufficient pressure in the reservoir is able to produce some of the oil, one have to keep in mind that the recovery is usually low. Oil production from primary recovery might range from 5-15% of OOIP (Enick and Olsen, 2012). To increase oil recovery, methods of Secondary Recovery is often introduced.

Secondary Recovery mainly cover two techniques, the injection of water/brine and the injection hydrocarbon gas to apply pressure support to the reservoir. Injection of water is commonly known as waterflooding and the method is well established within the industry and is often used and most effective in reservoirs where the water is the *wetting fluid*. In mentioned reservoirs, the rock formation prefer water to oil as the rock coating fluid along the pore walls and *Capillary forces* promote displacement by spontaneous imbibition, depending on the degree of wettability. Depending on the wetting nature of the rock formation and the capillary pressure of the reservoir, an injection of light component gases might be more effective. It is important to distinguish the use of hydrocarbon gas as a conventional oil recovery method and other gas injections that are categorized as EOR. Although both categories use gas injection to improve recovery, the injection of light gases in oil reservoirs is referred to as secondary recovery because the injection is used for pressure support. The injection of gas in EOR might be to alternate or optimize parameters such as viscosity, density, mobility or any of the other parameters that makes fluid flow, and ultimately production of oil, more effective. Secondary recovery methods have the capability to recover an additional 20-40% OOIP (Enick and Olsen, 2012).

1.2 Carbonate Reservoirs

The experimental work done for this thesis was performed on Edwards Limestones collected at an outcrop formation in Garden City, Texas. Carbonate rocks, Limestone and Dolomites, make up for approximately 60% of the world's oil and 40% of the world's gas (Schlumberger Market Analysis, 2007). Since the early 90's, extensive research has been conducted to improve predictions of performance in carbonate reservoirs, after the realization that more than 50% of the oil in place in most cases remained unswept after waterflooding, due to heterogeneity of the rock (Lucia et al., 2003). Carbonate reservoirs are highly heterogeneous in terms of pore geometry and are often naturally fractured.

This thesis is a part of the ongoing research being conducted for the U.S. field pilot research program. To understand and evaluate the exact properties of the reservoirs at East Seminole and Fort Stockton, Texas, one should work on core plugs drilled from those locations. However, drilling actual reservoir cores is expensive, thus it is common to work on outcrop cores with similar properties to be able to reproduce the desired conditions of the actual reservoir rock. In this thesis, the Edwards Limestone samples are considered replicates of the East Seminole, which is the carbonate reservoir of the two.

1.2.1 Heterogeneity

To some degree, all reservoirs are heterogeneous and a reservoir is said to be heterogeneous if it has significant variation in reservoir properties as a function of position or space within the reservoir. One of these reservoir properties is *porosity*, which is the storage capacity within the rock formation. Another is *permeability*, which is the parameter dictating at what ease and how effective a fluid can flow through the porous media. These two parameters are often used to demonstrate the level of heterogeneity present in a rock formation. Pore geometry can be expressed as the relationship between porosity and permeability, ϕ/K (Marzouk et al., 1998). Other properties that may be affected by heterogeneity are fluid saturations, wettability, pore size distribution and thickness of layers. Characterizing these reservoir properties and understanding the variations inflicted by heterogeneity is important when predicting the ability to store and produce hydrocarbons from the reservoir. In a limestone, the void space is characterized by a wide variation in shapes and distribution of pore sizes. Processes such as secondary solution, recrystallization, and fracturing distinctly affect the geometry of the porous systems and therefore yield high variations in pore shape pore size distribution (Craze, 1950). These variations give the limestone an uneven distribution of permeability and porosity.

1.2.2 Fractured Reservoirs

Natural fractures occur over time when a rock formation has been exposed to physical stress or diagenesis. Fractures can also be induced by human activity through drilling and hydraulic fracturing, i.e. used in tight shale oil production to enable fluid flow. Fractures range in size, from micrometers to several meters. Performance and production of a fractured reservoir is closely related to how the fractures dominate fluid capacity and flow in a reservoir. Fractured reservoirs are divided into four (which in will not be discussed under the scope of this thesis) groups based on the ratio of porosity and permeability, and how dominant the fracture is compared to the matrix of the rock formation (Allan and Sun, 2003). There are great challenges related to producing oil from fractured reservoirs. The fractures may exhibit permeabilities that are several orders of magnitude higher compared to the rest of the rock matrix. Therefore, injected fluids may easily channel through the fractures and thus

limit the build-up of differential pressure across the reservoir, resulting in poor sweep efficiency, early breakthrough and low recoveries (Haugen et al., 2010, Fernø, 2012). As for other fractured reservoirs, the matrix may have a more favorable porosity and permeability and in these situations, the fractures act as an enhancement to the production performance by easing the transportation of fluids to the production well (Allan and Sun, 2003).

1.2.3 Pore Size Distribution

Porosity and permeability are the two dominant factors determining the transmissibility in a rock formation. However, porosity and permeability measurements does not provide information about Pore Size Distribution (PSD), which is important when studying hydraulic flow behavior during fluid displacement. To better understand the behavior of fluid flow in carbonate reservoirs, it is common to introduce the concept of pore size distribution (Skauge, 2013). Figure 1.4 schematically illustrates an example of a rock formation with a uniform PSD, i.e. an equal number of all pore sizes.

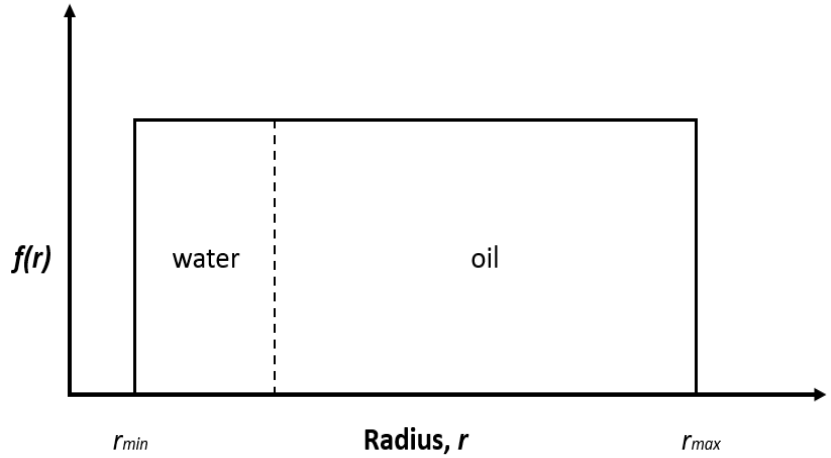

Figure 1.4: Pore size distribution as a function of pore radius for a typical water-wet reservoir. After primary drainage, water resides in the smaller pores, whereas the oil is present in the larger pores. The figure illustrates the distribution of pore radii in a rock formation. Reproduction of Figure 1.6 in *Pore Scale Physics and Network Modeling* by (Skauge, 2013).

The PSD is important because it affects the displacement behavior through the capillary pressure present in the rock formation. During the primary drainage of the reservoir, oil enters the largest pores and displaces water up to a critical radius (illustrated by the dotted line in Figure 1.4). This critical radius is of interest because it determines the phase occupancy of the pore depending on whether the radius is larger or smaller than the critical value. The oil saturation is calculated by summarizing the volume of pores filled with oil, divided by the total volume of all pores. Consequently, If the PSD is weighted towards an increase in number of pores that have radii larger than the critical value, the total oil saturation is increased compared to a uniform PSD. On the contrary, a PSD weighted toward an increased number of small pores with radii less than the critical value, oil saturation is decreased (Skauge, 2013). It is worth mentioning that rock formations with different PSDs and consequently different oil saturations, may yield the same measured values for porosity and permeability. This was apparent for some of the experimental work done in this thesis.

2. CO_2 Enhanced Oil Recovery and Mobility Control with Foam

This chapter discusses CO_2 mobility control and how foam can be applied to optimize mobility of the injected CO_2 as a measure for EOR. The chapter is starts with an introduction part covering main properties of CO_2 and surface active agents, continues with a general discussion of CO_2-foam and concludes with how mobility control of injected CO_2 may mobilize residual oil saturations in hydrocarbon reservoirs. Fundamental theory related to topics mobility, miscibility, capillary pressure, wettability, interfacial tension and permeability are found in Appendix II – Fundamental Parameters.

2.1 Properties of CO_2 and Surface Active Agents

CO_2 is a colorless and odorless molecule formed by one carbon atom and two oxygen atoms, bounded by two covalent polar double bonds. Even though the molecule has polar bonds, the molecule remains non-polar because the two dipole moments of the bonds cancel due to the linear geometry. CO_2 is an important greenhouse gas and make up for approximately 0,039 percent of the composition of air. CO_2 occurs naturally and as a product in every combustion where carbon is the source and to this day, the only mechanism known to decompose it is photosynthesis (Energy Institute, 2010). At standard temperature and pressure (T=15°C and P=1,013 bar) CO_2 is a gas, but with increasing temperature and pressure it will change phase into either liquid or supercritical fluid conditions. In the latter case, both temperature and pressure have to be equal or greater than a certain critical value. Pure CO_2 becomes supercritical state at conditions above 30,9°C and 73,8 bar (Farelas et al., 2012). Figure 2.1 is a phase diagram for CO_2 and shows pressure, temperature and corresponding phase behavior. In a supercritical state, it is difficult to determine if it is a gas or a liquid, because it acts as a fluid with properties of both. Thermodynamically, the density of a supercritical fluid is approaching that of a liquid phase, however, it is considered a gaseous phase because viscosity characteristics remains gas-like (Sidiq and Amin, 2010). Supercritical state behavior is chosen in this thesis because supercritical state CO_2 is reported to have doubled interaction with crude oil compared to gas state (Sasaki et al., 2013).

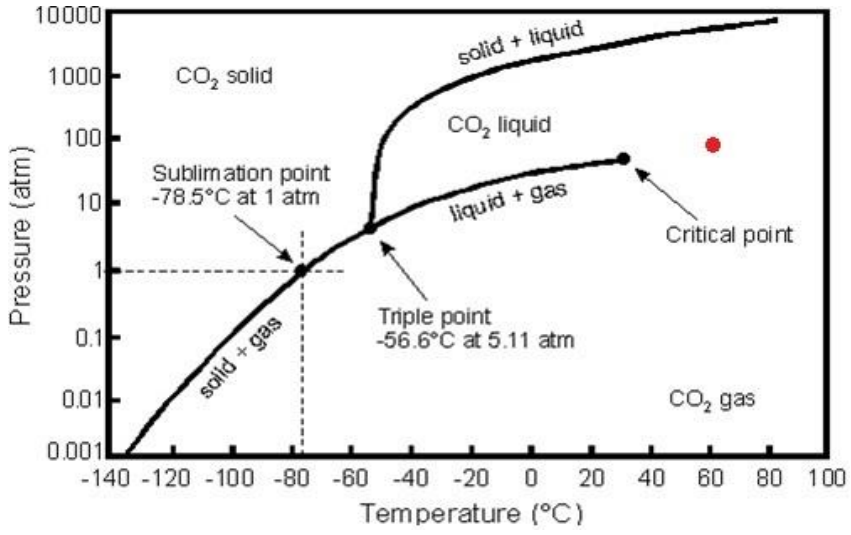

Figure 2.1: CO_2 phase diagram. The figure illustrates pressure, temperature and corresponding phase behavior. Four points are marked as dots, sublimation point (-78.5°C at 1 atm), triple point (-56.6°C at 5.11 atm) where CO_2 can co-exist as solid, liquid and gas, critical point (30.9 and 72.8 atm) and lastly the red dot, illustrating the conditions (60°C and ≈85 bar) and phase behavior of CO_2 in the experimental work for this thesis. The figure is obtained and modified from (Picha, 2007).

CO_2 may be applied in petroleum reservoirs as a secondary or tertiary process in a variety of injection strategies, WAG (Water Alternating Gas), SAG (Surfactant Alternating Gas), CGI (Continuous Gas Injection) or as a co-injection with another fluid. Regardless of how it is applied, CO_2 may contribute to improve oil recovery by interacting with the oil originally in place through effects of (Holm and Josendal, 1974, Mungan, 1981, Martin and Taber, 1992):

- Reduction of oil viscosity
- Increased oil density
- Swelling of oil
- Miscibility effects
- Increase of injectivity

The injection strategy discussed in this thesis will be the use of co-injection of supercritical state CO_2 and surfactant solution to generate mobility control foam. The CO_2-foam comprises of supercritical CO_2 and a foaming agent. The surfactant have the ability to lower the interfacial tension between two phases, which in this case with brine and CO_2, is essential for the generation of a stable mobility control foam. The surfactant must have one hydrophilic and one hydrophobic segment and for the foam to be stable the surfactant should be more soluble in water than in the CO_2 (Enick and Olsen, 2012). Foam stability is discussed in section 2.2.3. The hydrophilic part of the monomer will face towards the brine solution and the hydrophobic part will face the gas phase, and the concentration of monomers in the solution should be sufficient so that the Critical Micelle Concentration (CMC) is reached. The CMC is the lowest concentration at which surfactant monomers self-organize to form micelles, i.e. clusters of dissolved monomers. In order to reach desired properties for foam-generation and mobilization of oil, most surfactants must be at or above the specific CMC for the surfactant (Enick and Olsen, 2012).

2.2 CO_2-Foam

Mixing air, water and soap, generates a frothy substance referred to as foam. Foam consists of one continuous liquid phase, water and surfactant, and one discontinuous gas phase, air. Because foam is not thermodynamically stable, it will collapse when left undisturbed for a certain amount of time, leaving a clear water-surfactant solution behind. The same principles applies to CO_2-foams as well as familiar foams generated by the kitchen soap. The CO_2-foam will contain pockets of dispersed CO_2 separated by thin, liquid, almost sheet-like films, commonly referred to as *lamellae* (Enick and Olsen, 2012). Lamella is the barrier separating two gas bubbles and is the mechanism responsible for the generation and rupture of the foam (Zolotukhin and Ursin, 2000).

Although bulk foams and CO_2-foam might be similar in the aspect of physical properties, there are also important differences. The specific environment for foam used in porous media will differentiate CO_2-foam from bulk foams because of the size-range in which it operates. For example, in pipeline transport of bulk foams, several gas bubbles are dispersed across the cross-sectional area, whereas a pore within a hydrocarbon reservoir essentially only contain one gas bubble. Ransohoff and Radke proposed a definition that addresses the matter of size when considering foam, so from this point on foam in porous media will be defined as; an interconnected fluid comprised of stable lamellae with dispersed and discontinuous gas. Further, because the gas-bubbles inside a reservoir is in the size order of pore throats, interactions with pore walls will dominate the behavior of the foam flow as it propagates

through the reservoir (Ransohoff and Radke, 1988). Figure 2.2 illustrates the general structure of bulk foams where gas bubbles are dispersed and separated by liquid solution lamellae.

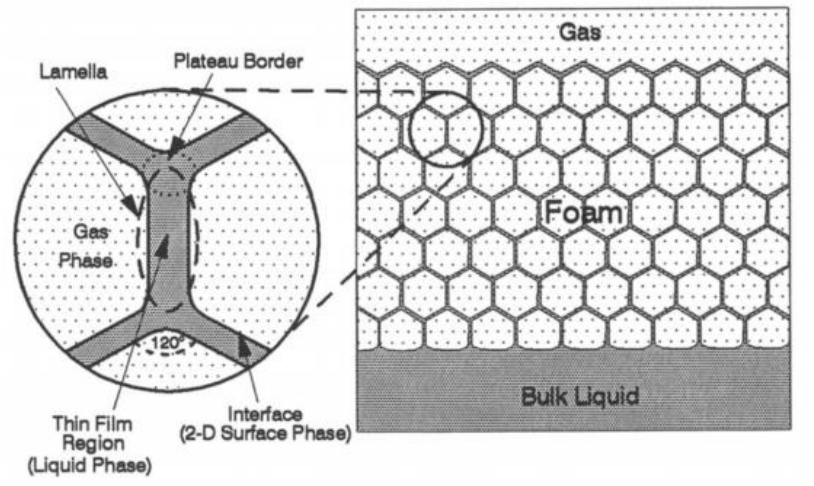

Figure 2.2: Basic structure of foam. The white-dotted gas-phase is dispersed in a foam structure separated by lamellae. The bulk liquid is visualized as the shaded phase at the bottom. The figure is obtained from (Schramm and Wassmuth, 1994).

2.2.1 Foam Generation

Understanding foam generation at pore level sizes is a comprehensive and difficult task. 2D and 3D observations of foam generation may visualize the mechanisms responsible and according to Ransohoff and Radke, three primary mechanisms for foam generation emerged from their study of foam generation in glass-bead packs: *Leave-behind*, *Snap-off* and *Lamella division*. These three mechanisms will be further discussed in this section. Leave-behind is the dominant mechanism if the velocity is below a certain value. Left-behind lamella is generated when two gas fronts invade adjacent liquid-filled pores. In this case, the liquid will be pushed in front and squeezed into a lamella dividing the two gas segments and generating a lamella oriented parallel to the flow. This is also called weak foam because the foam generation does not make the gas phase discontinuous, resulting in reduced pressure build-up (Ransohoff and Radke, 1988, Tanzil et al., 2002, Ward, 2016).

To understand the generation of foam from the effect of snap-off, it is important to understand how the pore geometry affect the pressure distribution. For this explanation, consider a gaseous phase invading a network of pores filled with a liquid phase, which also is the wetting phase. The pore neck or throat defines the pressure the gas-phase must overcome to enter, while the wider body of the pore defines the pressure for when the liquid re-enters the pore. When the gas approaches a pore throat it will gradually build up pressure at the gas-liquid interface until the curvature of the interface no longer can increase its arch. At this point, the gas will penetrate the throat and instantly displace the liquid. The whole pore will now be filled with gas, except the wetting film along the pore-walls. The displaced liquid will retreat all the way to the nearest pore throat when the curvature on the gas-liquid interface breaks. New interface and curvature between gas and liquid is created at the nearest throat that is narrow enough that a new pressure build-up in the gas-phase is required. Snap-off effects are observed to be more important for foam generation at higher pressures (Tanzil et al., 2002, Ransohoff and Radke, 1988). When a gas front is approaching a narrow constriction, such as a pore throat, snap-off occurs if the local capillary pressure at the constriction momentarily drops below the surrounding capillary pressure, allowing gas to invade the pore and liquid to accumulate at the constriction (Tanzil

et al., 2002, Rossen, 2003, Gauteplass et al., 2014). A liquid lens will be formed first and if the capillary pressure at the constriction rises again, it may bridge the throat and create a lamella that separates the gas bubble completely (Rossen, 2003, Enick and Olsen, 2012).

Lamella division is the last mechanism proposed by Ransohoff and Radke. The major difference between foam formation by division and the other two mechanisms is that lamella division is not generating gas bubbles, it is only subdividing existing mobile gas bubbles into new ones (Kovscek and Radke, 1993). Lamella division is therefore said to be a secondary foam generation mechanism (Ransohoff and Radke, 1988). Wherever a lamella reaches a branching point (site where one channel splits into two or more channels) inside the pore network, is where lamella division might occur and foam generation by division is highly dependent upon the number of branching points (also known as coordination number) inside the network. When a mobile lamella reaches a branching point two possibilities arises, the lamella can flow into two or more channels or into only one. In the former case, the foam lamella is generally of such size that it spans across the pore body and therefore it stretches across the branching point and enters new flow paths downstream, generating new gas bubbles. In the latter case, the lamella is either too small to span across all channels or an immobile gas bubble is blocking one or more of the paths, thus, no lamella division occurs (Ransohoff and Radke, 1988, Kovscek and Radke, 1993). Lamella division is similar to the snap-off mechanism in the sense that a separated gas bubble is created (Ransohoff and Radke, 1988). In the matter of mobility control, especially reduction of gas-mobility, both snap-off and lamellae division are suggested to be the most effective lamellae formation methods, because both effects has lamellae generation in the direction perpendicular to the flow of gas, particularly in constrictions such as throats (Enick and Olsen, 2012).

2.2.2 Foam Quality

Foams used in the industry are fitted into different categories depending on their properties and the area of operation. The different types of foam are developed into two main groups, *Mobility Control Foams* and *Conformance Control Foams*, where foam quality is the factor that differentiate the two. The foam quality is a measure of the gas to surfactant ratio. Foams that are generated to improve the mobility of the injected CO_2 to a level approximately equal to the mobility of the displaced oil are referred to as mobility control foams. These foams usually contain a dilute amount of surfactant and they are intended to last throughout the entire CO_2-flood, thus improving the macroscopic sweep profile. A dilute solution is preferable because a concentrated solution is not sustainable, the pressure build-up would be unmanageable. In addition, it would be wise to consider the economical side of the equation, because the amount of foam needed for a long-lasting flood would require a large volume of surfactant (Enick and Olsen, 2012). However, some situations promote the use of a highly concentrated surfactant solution. These foams are categorized as Conformance Control Foams and are usually generated with concentrated liquid surfactant solutions that are known to yield a good performance in high-permeability formations. This would generate a strong foam that can drastically increase the pressure build-up when injected in a high-permeability, watered-out, thief zone, which will alternate the direction of the injected CO_2 solvent to a more low-permeability, oil-rich region and ultimately increase the recovery. Conformance Control Foams can be injected to treat near-wellbore regions at injection and production wells (Enick and Olsen, 2012). The main difference between the two is that the purpose of a mobility control foam is to lower the mobility of the solvent used for displacement for the entire production, while a conformance control foam is a formation treatment as the foam is injected specifically to block high-permeable regions causing bypass of oil.

2.2.3 Foam Stability

Foams are used in a diverse range of applications and encounters a wide range of oil saturations. Several factors control the distribution of saturations in a petroleum reservoir prior to implementation of CO_2-foam; pore geometry, wettability, heterogeneity, fractures, production history (e.g. previous waterflood) and more. Proper designing and testing are thus necessary to ensure the stability of the foam. CO_2-foams are designed to perform in the specific environment in which they are supposed to operate. This section will elaborate the most important factors controlling foam stability. Factors relevant to the experimental work conducted in this thesis include liquid composition (surfactant and salinity), temperature and pressure.

Pressure affects the stability of CO_2-foam and the general trend is that elevated pressures increases its stability (Enick and Olsen, 2012). The density of CO_2 is increased with increasing pressure and the molecular interactions with liquid surfactant solution increases with increasing CO_2 density.

The liquid composition is important because the surfactant have to be soluble in the brine, while still interact with CO_2. A successfully composed liquid solution that exhibit good stability must contain the right concentrations of salt and surfactant. Salinity is a measure of the amount of salt dissolved in the water and depending on the brine salinity three different phase systems form. A Type II- system is a situation where the salinity is too low. In this system the surfactant may exhibit good solubility in the brine, but poor interaction with the CO_2, leaving an excess phase of pure CO_2. In a Type II+ system, the salinity is too high and stability of the CO_2-foam decrease due to the increase of electrostatic forces exhibited by the brine. At intermediate salinity a third system can form, Type III and excess phases of brine and CO_2 diminishes as a third microemulsion-phase form. This microemulsion-phase reduces the interfacial tension between the two phases, allowing both to combine into one phase (Zolotukhin and Ursin, 2000, Enick and Olsen, 2012).

The reservoir temperature is an important factor when considering the stability of CO_2-foam. It is apparent that the CO_2-foam stability decreases as it is exposed to increased reservoir temperatures due to the following (Handy et al., 1982, Noll, 1991, Enick and Olsen, 2012):

- Decrease of surfactant solubility in brine
- Thermal decomposition of surfactant
- Increase of Critical Micelle Concentration

The half-life of a surfactant (time until half of the surfactant has decomposed) has an exponential decrease as the temperature increases (Handy et al., 1982), which ultimately concludes all form of foam-generation. However, high temperatures can also promote a positive effect on foam stability. In a research done by Ziegler and Handy originally published in 1979, the conclusion was that surfactant adsorption decreased as the temperature increased. With the use of a non-ionic surfactant, they experienced that low concentrations gave a low rate of adsorption, while high concentrations increased the adsorption, as the temperature was increased (Ziegler and Handy, 1981). Reservoir temperature is an unalterable parameter during hydrocarbon displacement and the surfactant used to generate mobility control CO_2-foam at elevated temperatures requires proper screening and testing to ensure stability.

2.3 Mobility Control with CO_2-Foam

Tertiary gas injection projects on a worldwide basis are experiencing low recoveries due to macroscopic poor sweep efficiency and early break through, because of unfavorable mobility ratios between the gas and oil. Gravitational and viscous effects such as gravity override, segregation, channeling and fingering are the main phenomena that causes the gas to break through early. Gravity override and segregation are effects occurring because of insufficient density of the displacing fluid, which forces the densest fluid to fall to the bottom and the lightest to rise up by the effects of buoyancy and gravitation (e.g. segregated layers of gas, oil and water). Channeling is a viscous effect caused by heterogeneity in the reservoir and mobility differences between the displaced and the displacing fluid. The displacement front between the two fluids becomes unstable with increasing mobility differences and the displacing fluid tend to shoot through in regions of high permeability causing low sweep efficiency and early breakthrough. Fingering is also a viscous effect caused by mobility differences, more specifically, it is caused by severe differences in viscosity. Unlike channeling, it is somewhat indifferent to the grade of heterogeneity present in the reservoir. Fingering happens when the viscosity of the displacing fluid is very low compared to the displaced fluid. The displacing fluid will generate paths or "fingers" that propagate through the oil, using the path of lowest resistance all the way to the production well. These effects are more dramatic when injecting gas than in waterfloods because of the extreme gas-oil mobility ratio (Zolotukhin and Ursin, 2000, Farajzadeh et al., 2010).

The efficiency of any oil recovery is governed by the counteracting capillary and viscous forces present during a displacement. Capillary forces influences the snap-off entrapment of oil by pore geometry and wettability preferences, whereas the viscous forces enables mobilization of oil with applied pressure gradient and viscosity differences (Bashiri and Kasiri, 2011). The dimentionless ratio of viscous-to-capillary forces is referred to as the capillary number, N_{VC}, and is given by equation 2.1:

$$N_{VC} = \frac{\mu \cdot u}{\sigma \cdot \cos\theta} \qquad \textbf{2.1}$$

Where μ is the viscosity, u is the darcy velocity, σ is the interfacial tension between the displacing and the displaced fluid and θ is the wetting angle defining the wettability characteristics of the rock formation. The residual oil saturation trapped inside the porous media after fluid displacement is a function of the capillary number, with decreasing residual oil as capillary number increases. There are two ways of achieving increased capillary number. Either increase viscous forces or reduce capillary forces. The capillary forces can be reduced by injecting surfactant, which lowers the interfacial tension acting between the fluids present in the system. The viscous forces can be increased by injecting additives such as polymers, thickeners or by creating a foam which increases the apparent viscosity of the injected solvent. The latter case, with supercritical CO_2 as solvent, is what is intended in this thesis. Figure 2.3 illustrates the residual oil saturation as a function of capillary number, otherwise known as the Capillary Desaturation Curve (CDC). The range of a typical waterflood in terms of residual oil is shown in the figure. To enable further mobilization of trapped oil after the waterflood, the capillary number must increase by altering one or more factors that governs the capillary number.

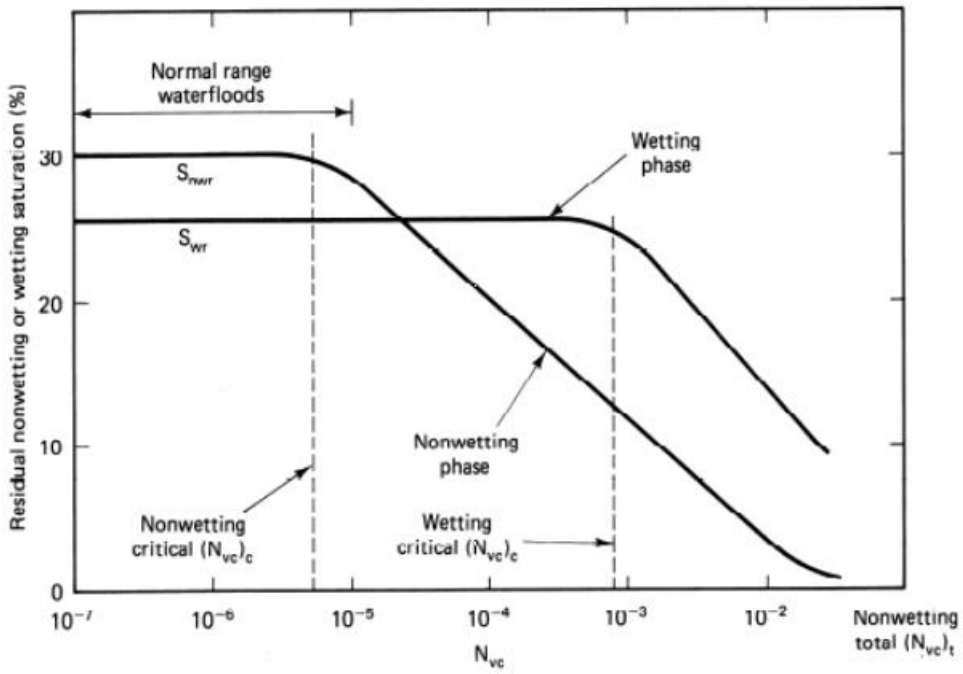

Figure 2.3: Residual oil saturation as a function of capillary number. Additional reduction of residual oil saturation after the waterflood is achieved if the capillary number is increased. Figure obtained from (Lake, 1989).

One offered solution to the problems caused by the low mobility of the injected gas is the mentioned simultaneous injection of surfactant solution to create foam, which mitigates the mobility differences between the gas and displaced oil, by increasing the apparent viscosity of the injected gas. A properly designed foam may reduce the gas mobility by several orders of magnitude and still keep the relative permeability unchanged, thus increasing the macroscopic sweep efficiency of the displacement and mobilizing residual oil saturations (Haugen et al., 2010, Zolotukhin and Ursin, 2000, Fernø et al., 2012)

CO_2-foam is labelled as "next-generation" CO_2-EOR and it is estimated that this EOR-method has the potential to add an additional 60 billion barrels of oil by utilizing larger volumes of CO_2, innovative flood designs and improving mobility control of the injected CO_2 (OFE, 2013). Petroleum reservoirs worldwide still hold a lot of residual capillary bound oil. This is backed up by the fact that the global average oil recovery is 22% (NPD, 2012). These reservoirs have often been subjected to conventional recovery methods through primary pressure depletion and secondary water or gas injection. The main disadvantage in primary recovery is that it yields a rapid decrease in reservoir pressure, which in turn leads to unacceptably low oil recovery. To support this disadvantage in pressure, secondary recovery via water or gas injection is often introduced. On the NCS, waterflooding is the most frequently applied recovery technique averaging a global-high oil recovery 46% (NPD, 2012). CO_2-foam may be a viable candidate for EOR on the NCS because it is likely that these reservoirs contain high-permeability, watered-out regions. Injected mobility control foam will generate pressure build-up in such regions, thus diverting the path of the displacement into low-permeable, oil-rich regions. As the CO_2-foam reach a low-permeability and oil-rich region, the foam will collapse at the leading edge, causing the pressure build-up to minimize, which enable sweep. Consequently, mobility control CO_2-foam modifies the entire macroscopic sweep profile of the reservoir by diminishing fluid flow in high-permeability regions and improving fluid flow and sweep in regions of low permeability (Farajzadeh et al., 2010).

3. Experimental Setup and Procedure

This part of the thesis describes the experimental procedures and setups used during the laboratory work. Information about core preparation, fluid and rock properties, experimental conditions, experimental design and strategy will be provided throughout this chapter. Routine core analysis includes the necessary core preparations required to conduct mobility control CO_2-foam floods. All experiments were conducted at the Department of Physics and Technology, University of Bergen.

3.1 Volumetric Change Parameter

During all experiments conducted with crude oil, a volumetric change parameter (VCP) is necessary to account for the change in volume due to applied pressures and temperatures. The VCP is a phase, fluid, pressure and temperature dependent variable, empirically determined for the relevant system. The VCP describes the volumetric change of the crude oil that occur as either higher pressure or higher temperature is introduced to the experimental system. The VCP can be calculated as the ratio of oil volume at reservoir conditions (RC) to the volume of oil at standard conditions (SC):

$$VCP = \frac{V_{O,RC}}{V_{O,SC}} \qquad \textbf{3.1}$$

In this thesis, the experimental work was conducted at approximately 85 bar and 60°C. The VCP was stepwise measured with a container filled with crude oil at three different conditions (Table 3.1) and the initial volume of crude oil in the container was 1000.00 ml.

- Condition A: temperature and pressure kept at standard conditions (1 bar and 20°C).
- Condition B: temperature increased, pressure kept at standard condition (1 bar and 60°C).
- Condition C: temperature and pressure at experimental conditions (90 bar and 60°C).

Table 3.1: Empirical test to determine Volumetric Change Parameter (VCP)

	Condition A	Condition B	Condition C
Abs. Pressure [bar]	1.00	1.00	90.00
Temperature [°C]	20.0	60.0	60.0
Volume [mL]	1000.00	1028.14	1002.81
VCP	1.000	1.028	1.003

*** Uncertainties: Pressure ±0,10%, Temperature ±0,1°C, Volume ±0,02 ml. The table is modified from experimental work done by PhD candidate Arthur Rognmo, University of Bergen.**

Crude oil volume increases as temperature increases, but decreases as additional pressure is applied and, as shown in Table 3.1, the volumetric effects by elevated temperature and pressure at experimental condition cancel, leaving a VCP of 1.003. Throughout the experimental work for this thesis the VCP has been regarded as 1.00 (note that it is only two digits), because uncertainties related to volumetric measurements of production exceeds the difference calculated by determining the VCP.

3.2 Rock Material and Fluids

In this section, fluids and rock material used are presented. Throughout the experimental work, 2'' diameter Edwards Limestone core plugs of varying lengths have been used. The cores are drilled out from blocks of rock formation collected from an outcrop in Garden City, Texas (Fernø et al., 2012). These outcrop rocks are highly heterogeneous in terms of pore geometry and reported to be strongly water-wet, thus, no wettability measurement has been conducted. Cylindrical samples are drilled using water to cool the drilling bit. Drilled cores are then dried in a heating cabinet at 90°C for at least 48 hours to remove any residual liquid saturation. Dimensions, bulk volume and weight are measured.

For the porosity and permeability measurements and the waterflood, a synthetic brine (ES-brine) is specifically made. All experiments were conducted on cores that initially was 100% saturated with ES-brine and then drained down to irreducible water saturation, S_{wi}, by injecting crude oil. In this thesis, all cores are assumed to be very water wet and the wettability-altering process related to exposing the cores to crude oil is neglected. The surfactant used for the CO_2-foam experiments is the same surfactant that is being implemented in the U.S. field pilot research program at East Seminole and Ft. Stockton. Table 3.2 lists fluids used with composition and associated properties at given conditions.

Table 3.2: Composition and thermodynamic properties of fluids used.

Fluid	Composition	Condition (T / P)	Density [c] [g/ml]	Viscosity [c] [cP]
ES-Brine [a]	22.796 mg/l NaCl 2.760 mg/l $MgCl_2$ $6H_2O$ 5.825 mg/l $CaCl_3$ $2H_2O$ 458 mg/l KCl	25˚C / 1 bar	0.940	≈1.00
Surfactant Solution	Huntsman Corporation SURFONIC®L24-22 NON-IONIC			
Multicomponent Ekofisk Crude Oil [b]	53 wt.% hydrocarbons 35 wt.% aromatics 12 wt.% resins 0.9 wt.% asphaltenes	20˚C / 1 bar 80˚C / 1 bar	0.849 0.85	14.3 2.7
CO_2-gas	>99.999 % CO_2	25˚C / 100 bar 60˚C / 100 bar 60˚C / 160 bar	0.818 0.290 0.638	0.074 0.024 0.050
Nitrogen gas [d]	>99.999 % N_2	25˚C	≈0.001	0.018

[a] ES-brine composition obtained from (Jian et al., 2015)

[b] Ekofisk Crude Oil composition obtained from (Graue et al., 1999) and (Fernø et al., 2012)

[c] Properties other than ES-brine, Ekofisk crude oil and Nitrogen are obtained from (NIST, 2011)

[d] Nitrogen properties obtained from Alicat Scientific Mass Flow Controller operating manual

3.3 Routine Core Analysis

The Routine core analysis is a repeated process and covers the necessary preparation before conducting the gas mobility control investigations. In routine core analysis, porosity and permeability for individual and stacked core systems were measured using procedures presented in sections 3.3.1 and 3.3.2. Core assembly and system pressurization are presented in section 3.3.3.

3.3.1 Porosity

Porosity was measured by saturating the core plugs with ES-brine and individually calculating the volume of brine in the core (V_p) to the bulk volume (V_b) of the core. Stepwise, this was done by inserting the cores into a container subjected to vacuum, preferentially lower than 100 mTorr (0.00013 bar). ES-brine was then injected into the container and left under vacuum conditions for 24 hours. After the saturation process, the cores were weighed again. The increase in weight after the saturation is caused by ES-brine entering and occupying the pore space. Figure 3.1 shows the weight difference principle.

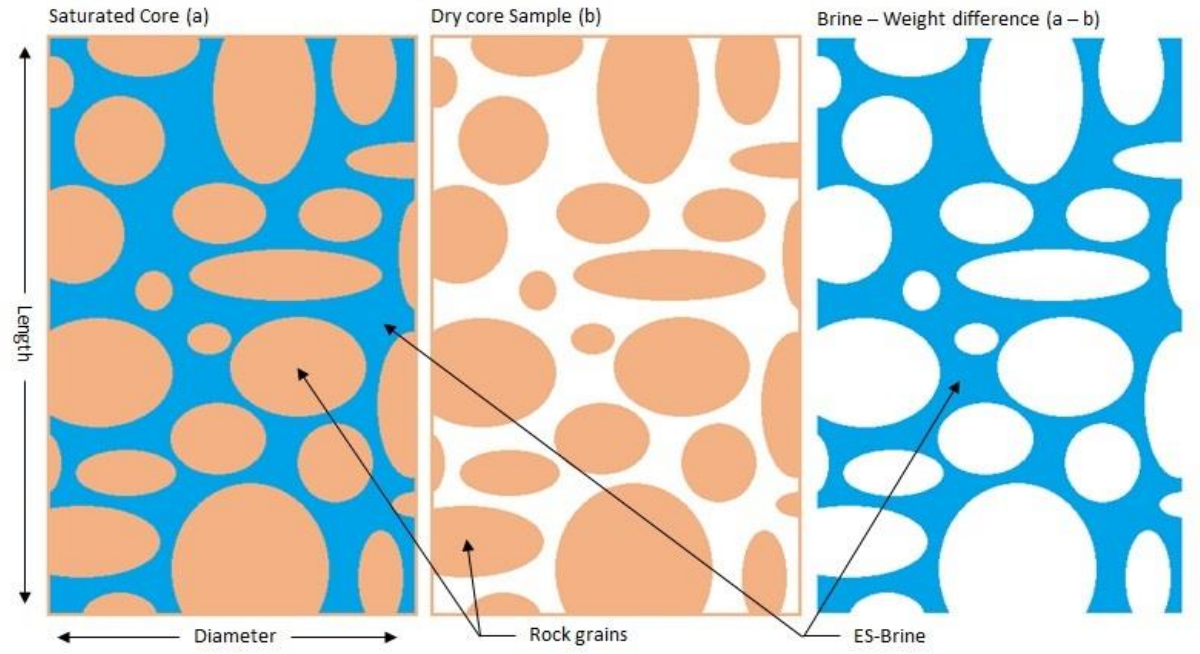

Figure 3.1: Breakdown of the principle behind the porosity measurement conducted. Before the core is saturated, it is weighed, and the weight difference before and after the saturation process is equal to the weight of the brine that has filled the empty space of the core during the saturation. Pore volume is calculated by dividing brine weight with its density.

$$\varphi = \frac{V_p}{V_b} = \frac{m_s - m_d}{\rho_b \cdot V_b} \qquad \textbf{3.2}$$

The weight of the brine in the core divided only by the density of the brine is a measure of pore volume and under the assumption that the core reaches 100% brine saturation after the saturation process, the porosity can be calculated with equation 3.2. m_s is the saturated weight, m_d is the dry weight, ρ_b is the density of the brine and V_b is the bulk volume of the core.

3.3.2 Absolute Permeability

Absolute permeability measurements were conducted on individual cores by using Darcy's Law, equation 3.3. When using Darcy's Law for absolute permeability, six requirements must be met. The core must to be 100% saturated with only the fluid used to measure permeability, the fluid must be incompressible and cannot chemically interact with the rock surface or alter the pore geometry and the flow must be laminar, stable and horizontal (Zolotukhin and Ursin, 2000).

$$Q = \frac{K \cdot A}{\mu} \cdot \frac{\Delta P}{L} \qquad \textbf{3.3}$$

Methodically, this was done by letting ES-brine flow through the core at a constant flowrate (Q) while measuring the differential pressure along the length of the core (dP). Because the cross-sectional area (A), the viscosity of the brine (μ) and the length of the core (L) are kept constant, the Darcy equation becomes quite easy to solve for the absolute permeability (K). The pressure reading was done several times at different flowrates and in both directions to increase accuracy. In this experiment 50 ml/h, 100 ml/h, 150 ml/h and 200 ml/h were used as fluid flowrates. An accurate permeability measurement should reflect a linear concurrence between the measured differential pressure and the applied flowrate, i.e. flowrate change should linearly affect the pressure measured. Figure 3.2 show the setup.

After the individual permeability measurements, the cores were paired in groups of four stacked cores. Because of the heterogeneous nature of this rock in terms of permeability, each stacked core system consists of cores with similar permeability. The succession of cores in the stacked system was noted and kept unaltered for the remainder of the experimental work (permeability may vary if the order is changed between experiments). The same setup (Figure 3.2) was used for stacked core measurements.

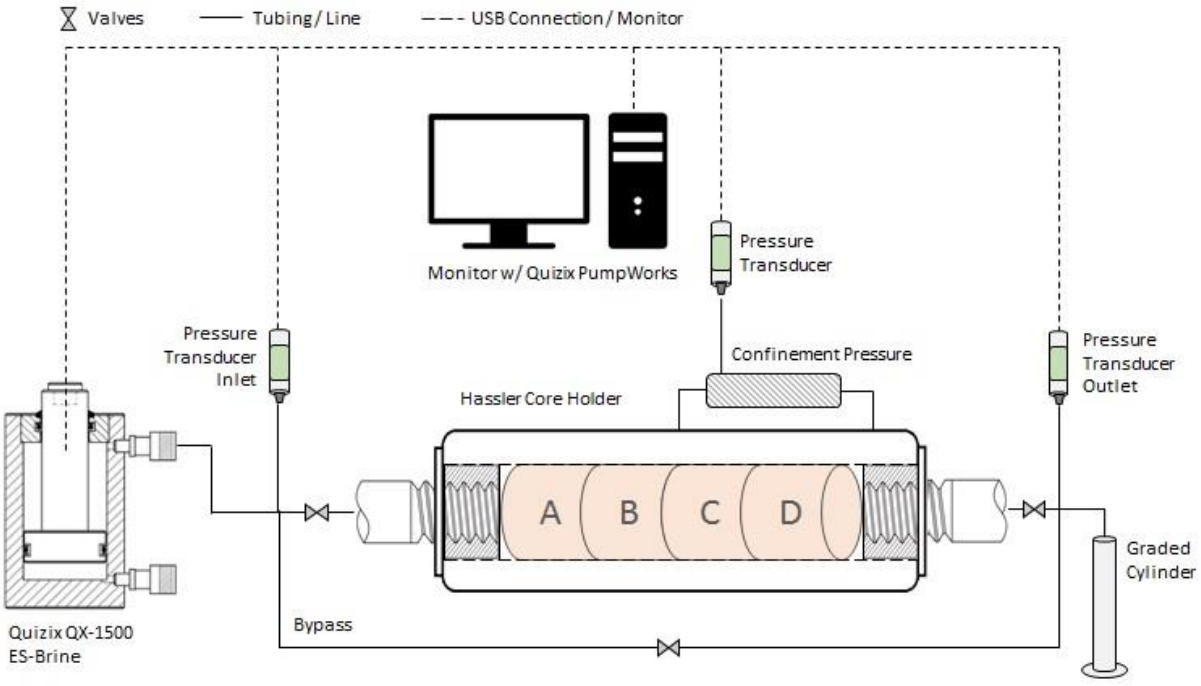

Figure 3.2: Illustration of the laboratory setup used for individual and stacked core absolute permeability measurements. The Hassler core holder was modified for respective individual or stacked core absolute permeability measurement.

3.3.3 Core Assembly and System Pressurization

After porosity and permeability measurements, the next step was to prepare the cores for the mobility control investigation. Paired cores were assembled in the correct order from the injection side (Inlet) to the production side (Outlet). The cores were wrapped in aluminum foil to prevent any fluid from flowing out of the core. After the stacked cores were wrapped, the tubing line end-pieces were placed on each end and attached with aluminum tape. Aluminum was used because CO_2 is a highly corrosive gas and may damage the encapsulating rubber sleeve inside the Hassler core holder. Lastly, the stacked cores along with the end-pieces were inserted into the Hassler core holder and fastened.

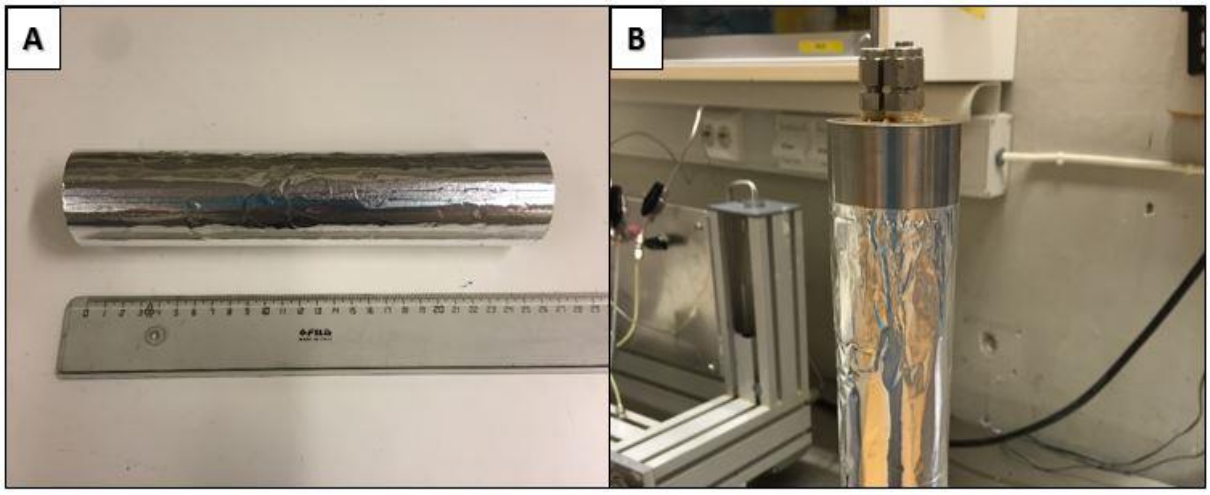

Figure 3.3: A) Stacked system of four individual cores wrapped in aluminum. B) Injection side and production side tubing line end-pieces are mounted on each side of the stacked core and fastened with aluminum tape. Aluminum is used to prevent any CO_2 to come in contact with and damage the confining rubber sleeve inside the Hassler core holder.

After mounting the cores in the Hassler core holder and applying confinement pressure, ES-brine was set to continuously pump through the cores and out to a production cylinder to flush out any remaining bubbles of air that might have been trapped during the saturation process. The system pressurization was done by applying nitrogen gas (N_2) to the Back Pressure Regulator (BPR, See figure 3.4), which is the device controlling liquid production pressure. The system pressure was approximately 85 bar, with a slight variation for each experiment. The flow regulator on the N_2-tank behaved sensitively when making adjustments above 50 bar and made it difficult to obtain precisely 85 bar for all experiments.

3.4 Mobility Control

This subchapter presents procedures for the CO_2-foam floods and the baseline test. In total, three mobility control CO_2-foam experiments and one baseline CO_2/ES-Brine co-injection was conducted. All experiments was performed using the same setup. Cores were assembled as described in section 3.3.3, and placed vertically in the heating cabinet. Figure 3.4 is a schematic illustration of the experimental setup used during primary drainage, waterflood and the mobility control investigations. All experiments described were done in collaboration with PhD candidates Sunniva Brudvik Fredriksen and Zachary Paul Alcorn, with occasional contribution from fellow MSc student Connie Wergeland.

3.4.1 Experimental Setup

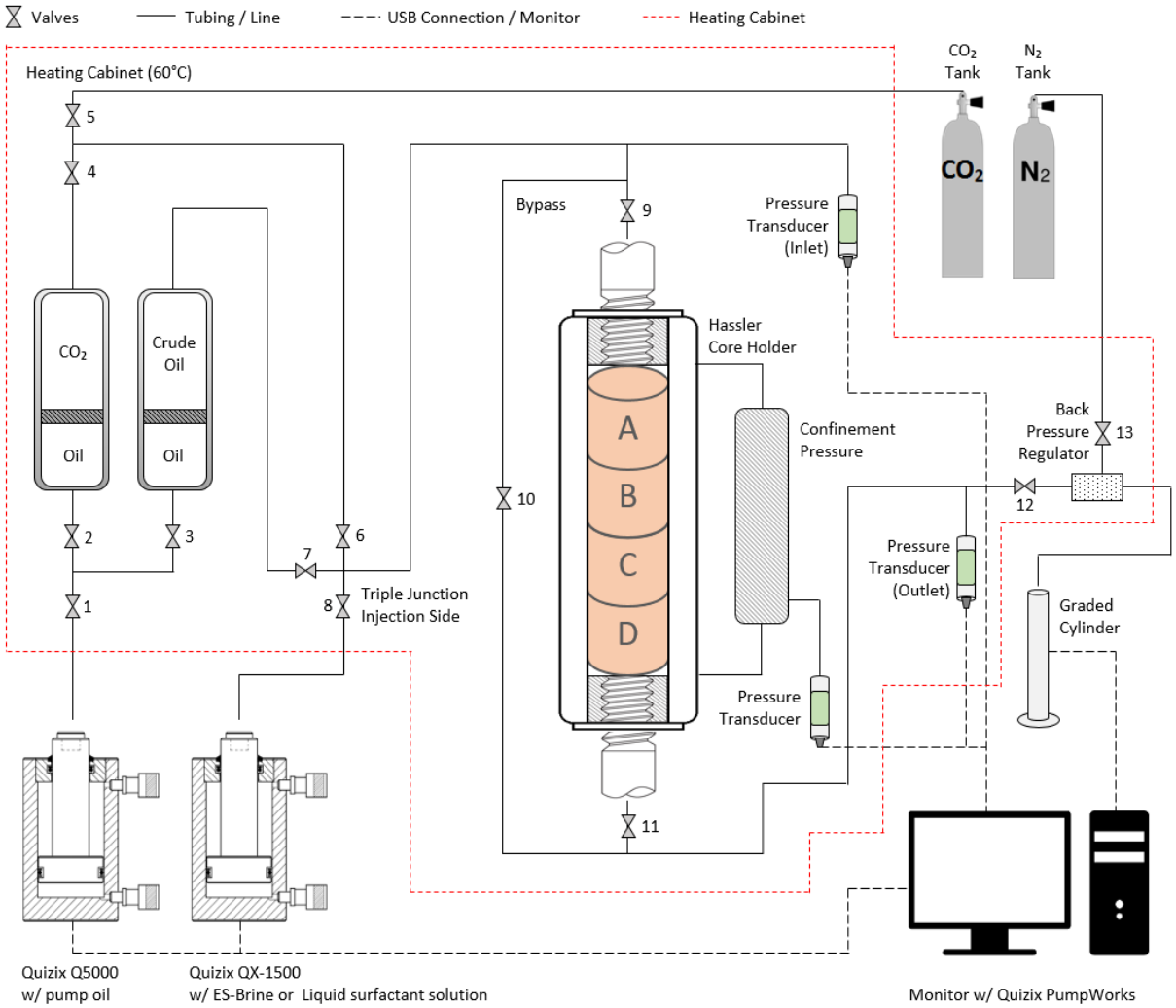

Figure 3.4: Schematic illustration of the high-pressure setup for the supercritical CO_2-foam mobility control experiments. The enclosed red-dotted line represents the heating cabinet, black-dotted lines are the communication cables connected to the computer and the solid black lines are the tubing lines carrying fluid flow.

Prior to all experiments conducted using this setup, the piston accumulators (crude oil and CO_2) were pressurized and stabilized at the desired experimental conditions (≈85 bar and 60°C). CO_2 is assumed to operate within the supercritical region and to interact with the crude oil through multiple-contact miscibility (cf. Appendix II – Miscibility). The pressurization was done by applying N_2-gas to the BPR and carefully flowing ES-brine through the bypass, until the system pressure stabilized. Confinement pressure was always kept 20 bar above system pressure to prevent any fluid from flowing between the sleeve and the stacked cores. In the following sections, detailed descriptions of procedures used during the primary drainage, waterflood, CO_2-foam flood and baseline will be presented. Numbered valves are included in these descriptions and can be found in the experimental setup illustrated in Figure 3.4.

3.4.2 Apparatus

The list of equipment listed below is the same as what is visualized in Figure 3.4. This is the constituents of the experimental setup:

- Quizix Q5000 Series Pump System
- Quizix QX-1500 Pump System
- 2x ESI 250bar Pressure Transducer
- Heating Cabinet
- 2” diameter Hassler Core Holder
- 2x Stainless Steel Piston Accumulator
- 2x Safety valves (120/160 bar)
- N_2 tank (Max. pressure 190 bar)
- CO_2 tank (Max. pressure 60 bar)
- Equilibar Precision Back Pressure Regulator (BPR)
- Computer operating pumps and monitoring line pressure
- Swagelock 1/8” diameter steel tubing lines, fittings and valves
- Graded production cylinder

3.4.3 Primary Drainage

Primary drainage is the process where the non-wetting phase displaces the residing wetting phase inside a porous media. In this case, crude oil displaces ES-brine in a porous system of four stacked heterogeneous Edwards Limestone core samples. Capillary pressure is the parameter that influence the drainage. In a heterogeneous system, the largest pores will be drained first because it requires the least amount of capillary entry pressure to overcome. As the phase-pressure of the crude oil is increased, smaller and smaller pores are drained and ultimately establishes the initial oil saturation.

Before the primary drainage, the stacked cores were mounted into the hassler core holder, which was placed inside the heating cabinet. The drainage process was performed using the experimental setup illustrated in Figure 3.4 and the system was pressurized as described in section 3.3.3. The crude oil-accumulator was completely filled with crude oil (850 ml) and all parts needed to conduct the primary drainage were left for 24 hours of heating at 60°C. The primary drainage was set to inject with a differential pressure of 2 bar per centimeter of core (approximately 50 bar above system pressure). The computer operated the pump and monitored pressure differential across the stacked core system. Confinement pressure was applied and continuously kept 20 bar above the pressure monitored at the injection side. The drainage lasted until at least 3.0 PV of crude oil was injected. Brine production was

continuously measured during the drainage and the amount of brine displaced by crude oil represents the amount of oil that has entered the stacked cores, corrected by the VCP described in section 3.1. After the drainage process, the core holder was isolated (valves 9 and 10 closed) when the pressure was approximately 85 bar. Because only crude oil was used, the piston accumulator containing CO_2 (left hand side) and the Quizix QX-1500 with ES-Brine (Bottom left) were closed off the system.

Because cores exposed to crude oil start an aging process, the primary drainage was conducted within 24 hours prior to the waterflood. If left saturated with crude oil for too long, the aging process will eventually alter the wetting characteristics of the stacked cores. The heterogeneous nature of Edwards Limestone causes the previous strongly water-wet porous media to become a mixed-wet media (cf. Appendix II – Wettability), which complicates further investigations. This aging process is assumed negligible. The primary drainage establishes the initial oil saturation in the stacked core systems.

3.4.4 Waterflooding

Waterflooding was performed on all stacked core experiments. This was intentional and necessary, because the U.S. field pilot research program includes depleted reservoirs that have been waterflooded for decades. Some of these reservoirs are carbonates and will likely have some high-permeability, watered out zones that are targets for CO_2-foam. To reproduce the actual environment and to see what effects the mobility control CO_2-foam might have, waterflooding was therefore included in all four experiments. The waterflood was performed by injecting ES-brine from the Quizix QX-1500 pump at 10 ml/h. The waterflood was conducted using the following experimental procedure:

Step 1: Ensured that the Hassler core holder was isolated after the drainage process

Step 2: The tubing lines were flushed with mineral oil (n-Decane) and N_2-gas to rinse the system for any crude oil present after the drainage process

Step 3: ES-brine was pumped through valve 8 (ES-brine tubing line at triple junction) and into the tubing lines through the bypass

Step 4: Ensured that the system pressure had stabilized at approximately 85 bar

Step 5: ESI-Pressure transducer software logging was started

Step 6: Quizix PumpWorks software logging was started

Step 7: Closed valve 10 (bypass)

Step 8: Opened valves 9 (inlet), 11 (outlet)

Step 9: Cumulative Volume Injected recorded at the Quizix QX-1500 pump were noted

Step 10: Time of start was noted

During the waterflood, liquid production was recorded. A graded cylinder accumulated the total production and the amount of crude oil accumulated was calculated by subtracting ES-brine production from the total production. 1.0 PV of ES-brine was injected (approximately 12 hours) during the waterflood before the Hassler core holder was isolated (valves 9 and 11 closed) and the fluid flow was diverted back into the bypass (valve 10 opened).

3.4.5 Co-injection

The waterflood concludes the repeated steps each of the stacked core systems have undergone. This chapter describe the experimental procedures for mobility control CO_2-foam floods and co-injection of supercritical CO_2 and ES-brine. Table 3.3 provides an overview of the experimental injection strategy for each experiment. The same experimental procedure was used for the foam floods and the baseline.

Table 3.3: Experimental overview including type, strategy and rates for respective stacked core system.

Stacked Core ID	Experiment Type	Experiment ID	Injection Strategy	Gas Inj. Rate	Liquid Inj. Rate
E-12-19-22-23	CO_2-Foam	CO2F2	Co-Injection (CO_2/Surf. Sol.)	8 ml/h	2 ml/h
E-9-18-21-11	CO_2-Foam	CO2F3	Co-Injection (CO_2/Surf. Sol.)	8 ml/h	2 ml/h
E-25-24-27-28	CO_2-Foam	CO2F4	Co-Injection (CO_2/Surf. Sol.)	9 ml/h[b]	1 ml/h[b]
E-13-16-14-15	Baseline[a]	BL1	Co-Injection (CO_2/ES-Brine)	8 ml/h	2 ml/h

[a] The experiment conducted as a non-foam co-injection of supercritical CO_2 and ES-brine is referred to as the baseline.
[b] Note that the foam quality is increased to 90% for the experiment conducted in CO2F4.

The co-injections were conducted using the following experimental procedure:

Step 1: Ensured that the Hassler core holder was isolated after the waterflood

Step 2: Ensured that the Quizix QX-1500 pump was filled with surfactant solution at 85 bar

Step 3: Ensured that the CO_2 piston accumulator was filled and stabilized at 85 bar

Step 4: Ensured that the system pressure was stabilized at approximately 85 bar

Step 5: ESI-Pressure transducer software logging was started

Step 6: Quizix PumpWorks software logging was started

Step 7: Quizix QX-1500 was set to inject at 2 ml/h (1 ml/h in CO2F4)

Step 8: Quizix SP5200 was set to inject at 8 ml/h (9 ml/h in CO2F4)

Step 9: Closed valve 10 (bypass)

Step 10: Opened valves 8 (Surfactant or ES-brine tubing line) and 6 (CO_2 tubing line)

Step 11: Opened valves 9 (inlet) and 11 (outlet)

Step 12: Cumulative Volumes Injected at both pumps were noted

Step 13: Time of start was noted

In this thesis, three experiments were conducted to study recovery by the use of CO_2-foam for mobility control under supercritical conditions. The CO_2-foam was generated in-situ (no foam generator used) by co-injecting supercritical CO_2 and surfactant solution. All co-injections were conducted using 10 ml/h total injection rate (individual gas and liquid injection rates are described in table 3.3). During the co-injections, liquid production was recorded and accumulated crude oil production was calculated by subtracting total water production from the total production. The co-injections were concluded after approximately 2.0 PV injected. After the co-injections, ES-brine was pumped through the system at a low rate to monitor the line pressure while depressurizing the system (releasing N_2-pressure at BPR).

3.5 Numerical Simulation

Numerical simulation has been conducted using the Eclipse Simulation Launcher to history match results and to conduct sensitivity parameter studies based on experimental work done at the laboratory. All simulations and sensitivity studies were based on a template simulation data file and specific grid built by PhD candidates Zachary Paul Alcorn and Mohan Sharma, University of Bergen.

Eclipse is a simulation engine owned by Schlumberger and it is used in relation to evaluate and interpret physical properties and phenomena through numerical modeling, with the ability to project future performance. The numerical process includes subdividing the desired reservoir into a model of several discrete cells of three dimensions and calculating several equations projecting the fluid flow behavior and material balance over each time step recorded (SLB, 2014). There are two options available in the Eclipse simulator suite: *ECLIPSE100* and *ECLIPSE300*, where E100 is referred to as the black oil simulator, whereas the E300 is the compositional fluid simulation software (Melby, 2014). The E100 assumes that oil and gas is one component and that this component can change in time by change in pressure and temperature, whereas the E300 is a comprehensive and component sensitive engine that tracks each component specified (C_1, C_2,…, C_n). The multi-component engine assumes that the oil and gas compositions can be represented by an equation of state under various conditions (SLB, 2014). All simulation done in this thesis has been conducted on the E100 Black Oil simulation software.

The purpose of the numerical simulation done in this thesis was to reproduce results from the experimental work done at the laboratory. Measured production (crude oil and brine) was evaluated and subsequently inserted in the simulator along with measured core-specific values such as core dimensions, porosity, permeability, initial oil saturation at given experimental conditions. Simulation time steps was set to the actual time steps where liquid production was measured at the laboratory.

The grid dimensions were set to be 1 * 1 * 400 in *X*, *Y* and *Z* directions, respectively and the grid consists of two saturation regions (SATNUM keyword), cells of core material and cells of spacing between cores, which is visualized by the orange and blue colors, respectively in Figure 3.5. Although, SATNUM was defined for both core material and spacing, the base model was set to have equal initial oil and water saturations in all cells, meaning that the spacing between the cores is regarded as core material as well. Two wells were added to the base model using the WELLSPECS and COMPDAT keywords, one injector perforated in the first grid cell (1, 1, 1) and one producer perforated in the last cell (1, 1, 400).

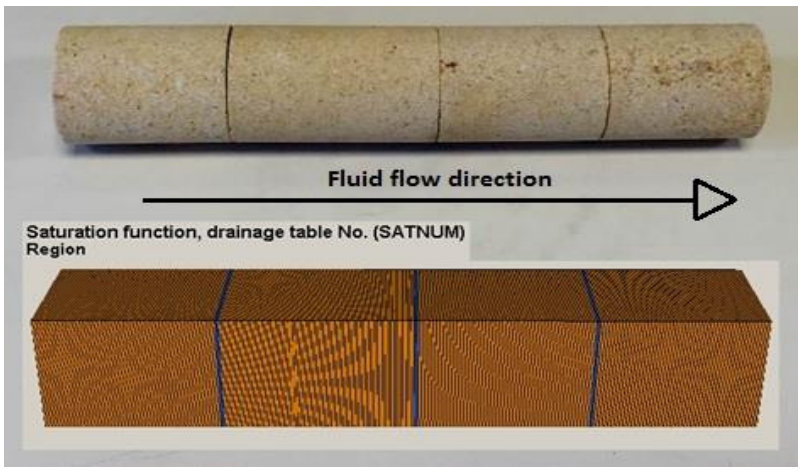

Figure 3.5: Top: Stacked system of four Edwards Limestone core samples. Bottom: Grid for the simulated base-model.

4. Results and Discussion

Experimental results and accompanying discussion are presented in this chapter. A total of 28 cores were prepared for the experimental work. The mobility control investigations on stacked core systems were conducted as three tertiary mobility control CO_2-foam experiments and one non-foam baseline co-injection using CO_2 and ES-Brine. This chapter starts with an overview of basic core data obtained from the routine core analysis, followed by an overview of experimental results and observations.

4.1 Routine Core Analysis

Core properties measured as described in subchapter 3.3. This subchapter provides two tables, one for individual core data (Table 4.1) and one describing properties of stacked core systems (Table 4.2).

Table 4.1: Individual core data obtained from routine core analysis.

Core ID #	Length [cm] ± 0.01	Diameter [cm] ± 0.01	Bulk Volume V_b, [ml] ± 0.05	Pore volume V_p, [ml] ± 0.37	Porosity [φ] ± 0.01	Permeability **(Abs.)**, [mD] ± 0.03
E1	5.90	4.94	113.08	37.71	0.33	63.86
E2	5.80	4.95	111.62	36.27	0.32	37.36
E3	5.77	4.95	111.04	36.28	0.33	49.10
E4	6.30	4.98	122.71	32.35	0.26	38.25
E5	5.89	4.95	113.35	31.84	0.28	16.01
E6	8.01	4.97	155.39	38.26	0.25	60.47
E7	5.48	4.97	106.31	31.12	0.29	50.57
E8	6.00	4.96	115.93	33.86	0.29	16.72
E9	6.13	4.97	118.92	30.40	0.26	34.80
E10	6.15	4.97	119.31	29.60	0.25	25.09
E11	6.24	4.97	121.06	31.52	0.26	37.82
E12	6.20	4.96	119.80	31.81	0.27	43.95
E13	6.14	4.97	119.12	31.23	0.26	64.53
E14	6.09	4.96	117.67	30.69	0.26	53.50
E15	5.80	4.97	112.52	28.48	0.25	47.41
E16	6.06	4.97	117.56	31.71	0.27	62.34
E17	6,01	4.97	116.59	30.11	0.26	50.95
E18	6,09	4.96	117.67	30.33	0.26	34.91
E19	6,08	4.97	117.95	31.34	0.27	43.60
E20	5.41	4.96	104.53	27.73	0.27	44.41
E21	6.17	4.97	119.70	30.78	0.26	35.11
E22	6.03	4.97	116.98	30.81	0.26	43.88
E23	6.12	4.97	118.73	30.94	0.26	39.71
E24	6.19	4.97	120.09	30.84	0.26	37.11
E25	6.17	4.97	119.70	30.95	0.26	37.92
E26	6.12	4.97	118.73	30.56	0.26	43.25
E27	6.02	4.97	116.79	29.19	0.25	32.63
E28	6.05	4.97	117.37	29.65	0.25	32.64

As proposed by (Marzouk et al., 1998) and mentioned in Section 1.2, the heterogeneous nature of the rock formation can be demonstrated by the relationship between porosity and permeability. As Table 4.1 shows, 28 carbonate core plugs were prepared and porosities and permeabilities ranged from 24,62% – 33,35% and 16,01 mD – 64,53 mD, respectively. Figure 4.1 compares the cores prepared for this experimental work and previous work done on the same core type by (Hjartnes, 2015) and (Haugen et al., 2014). Measured porosity showed a relative consistency in the majority of the cores prepared, making the wider range in permeability the decisive factor that determine heterogeneity. However, a general trend is observed and it is evident that increasing porosity entails an increase in permeability.

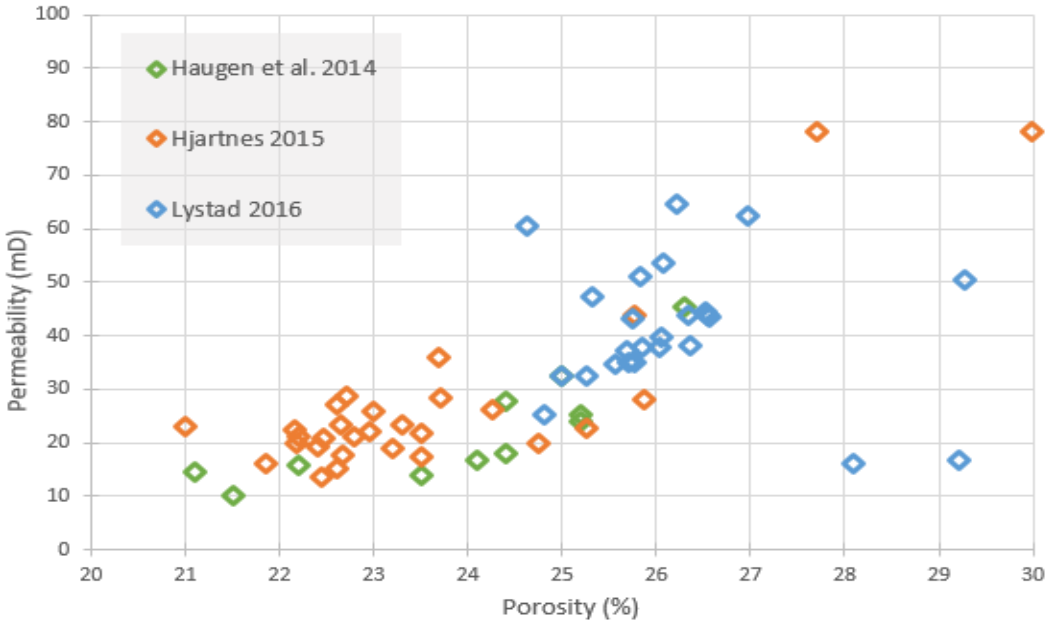

Figure 4.1: Permeability and porosity measured in this thesis matched with available literature data from (Hjartnes, 2015) and (Haugen et al., 2014). Porosity measured for the majority of the cores prepared show a relative narrow range, 24 – 27%, whereas the permeability vary between 25 – 65 mD.

After grouping individual cores of similar properties in stacked systems of four cores, permeability measurements and primary drainage are conducted as described in sections 3.3.2 and 3.4.3. The length of the stacked core system, bulk volume, pore volume and corresponding porosity are calculated directly from the individual core data (see Table 4.2). Changes in properties added by the presence of the spacing in-between the cores, are neglected. It is assumed that the permeability measurements are unaffected by the spacing because the spacing is perpendicular to the direction of the fluid flow.

Table 4.2: Properties measured for the stacked core systems.

Stacked Core ID #	Experiment Type	Exp. ID #	Length [cm] ± 0.04	V_b [ml] ± 0.09	V_p [ml] ± 0.81	Poro. [φ] ± 0.02	Perm. [mD] ± 0.21	S_{wi} [0-1] ± 0.01
E-12-19-22-23	CO_2-Foam	CO2F2	24.43	473.46	124.89	0.26	25.02	0.25
E-9-18-21-11	CO_2-Foam	CO2F3	24.63	477.35	123.03	0.26	26.92	0.37
E-25-24-27-28	CO_2-Foam	CO2F4	24.43	473.94	120.63	0.25	28.50	0.23
E-13-16-14-15	Baseline	BL1	24.09	466.87	122.12	0.26	45.49	0.29

4.2 Results Overview

In this section, experimental results from the mobility control investigations are presented. Table 4.3 provides an overview of initial oil saturation, recovery obtained from waterflood, additional recovery from co-injection and total recovery for each experiment that was conducted. Individual results from the mobility control CO_2-foam experiment and the baseline co-injection are presented in section 4.3.

Table 4.3: Overview of experimental results.

Stacked Core ID #	Experiment Type	Experiment ID #	Initial Oil Saturation $S_{o,iw}$ [0-1]	Waterflood Recovery [%]	Co-injection Recovery [%]	Total Recovery [%]
E-12-19-22-23	CO_2-Foam	CO2F2	0.75	49.9	22.2	72.1
E-9-18-21-11	CO_2-Foam	CO2F3	0.63	62.9	17.2	80.1
E-25-24-27-28	CO_2-Foam	CO2F4	0.77	53.5	15.7	69.3
E-13-16-14-15	Baseline	BL1	0.71	57.2	29.8	87.0

4.2.1 Primary Drainage

It is apparent that the heterogeneous nature of Edwards Limestone causes a variation in the initial oil saturations obtained. The assumption made prior to primary drainage was an initial oil saturation of approximately 0.75 fractions of total pore volume (this was based on personal conversation with PhD candidate Sunniva Brudvik Fredriksen) and that all stacked cores were equally water-wetted (cf. Section 3.1). Stacked cores CO2F2, CO2F4 and BL1 ranged between 0.71 and 0.77, compared to only 0.63 for CO2F3. The observed low initial oil saturation in CO2F3 may derive from pore-scale physics during primary drainage and unbalanced pore-size distributions, PSD. First, the physical principle that drives primary drainage is the capillary entry pressure. Each pore has an associated entry pressure defined by the size of the pore, more specifically, the radius of the pore throat (Equation A.3, Appendix II). As pressure is applied to the crude oil, it will enter the largest pores first because it requires the least amount of pressure to overcome. Subsequently, smaller and smaller pores are drained up to the point where the applied pressure is no longer sufficiently high enough to exceed the present capillary pressure. In a uniform PSD, such as the one illustrated in figure 1.5 (cf. Section 1.2.3), this is where the drainage reaches its potential. However, a pore large enough to be drained can remain 100% brine saturated for two reasons, based on theory known as Invasion Percolation. The pore is either *inaccessible*, i.e. there exist no neighboring pore already filled with oil, or the brine residing within the pore is *trapped*, i.e. portions of brine hydraulically disconnected from the chain of brine-filled pores being drained (Skauge, 2013). Secondly, the PSD is rarely uniform and may cause variation in observed initial oil saturation if the stacked core systems have significantly different PSDs. I urge the reader to revisit section 1.2.3 for elaboration on pore-size distribution. The smallest pores, that have a capillary entry pressure too high for crude oil to enter, will remain 100% brine saturated. Edwards Limestone is assumed to be highly heterogeneous in terms of pore geometry and if CO2F3 experienced a PSD weighted towards an increased number of small pores compared to the other stacked cores, a reduced initial oil saturation is justifiable. It is suggested that the variation in initial oil saturations observed for the cores may derive from unbalanced PSDs and effects of inaccessibility and immobilized brine.

The mobility experiments were designed to investigate oil recovery by co-injection of supercritical CO_2 and surfactant solution. All of the stacked core systems were initially 100% saturated with ES-brine and drained to initial oil saturation with crude oil. Waterflooding was performed in all experiments, followed by either co-injection of supercritical CO_2 and surfactant solution or co-injection of supercritical CO_2 and ES-Brine (Baseline). Figure 4.2 shows each successfully conducted experiment and the respective total oil recovery as a function of pore volumes injected. Figure 4.2 represents reproductions of measured values and serves to provide basic information about oil recovery only. All experiments conducted are individually presented in section 4.3, providing a detailed discussion of observations made during the CO_2 mobility control investigations.

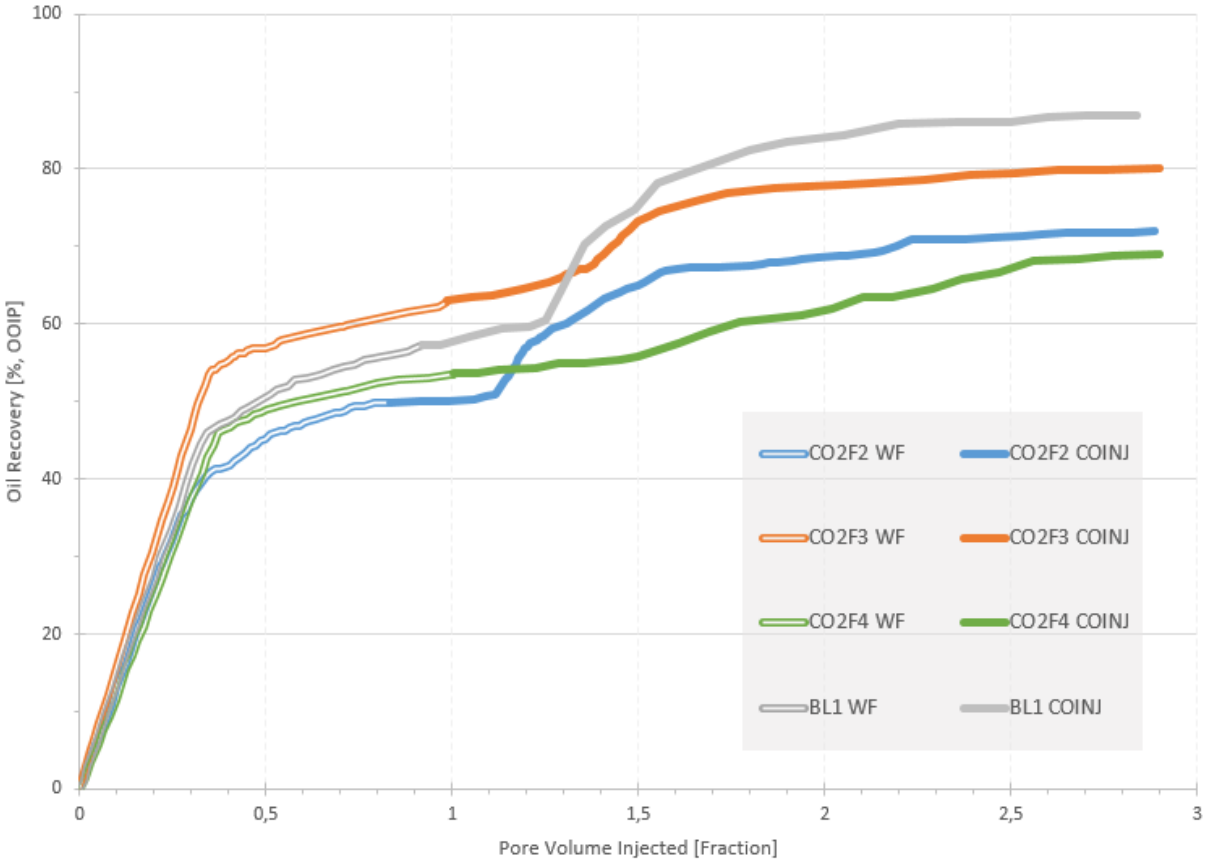

Figure 4.2: Overview of total recovery versus number of pore volumes injected. The lines illustrate the estimated oil recovery at given value of PV injected. Experiment ID is described in the color legend. The doubled lines represents recovery by waterflood (WF) and the solid lines represents recovery by co-injection (COINJ) of both supercritical CO_2/ surfactant solution (CO2F2-CO2F4) and supercritical CO_2/ES-brine (BL1).

4.2.2 Waterflood

Waterflooding was performed for approximately 1.0 PV injected and the amount of PV injected before two-phase production was relatively consistent for the stacked cores (0.35 PV injected), whereas the oil recovery vary between 49.9% and 62.9% OOIP. The performance of the recovery during the waterflood is dependent on the initial oil saturation. As expected, the total oil recovery from CO2F3 was high because of the low initial oil saturation observed (0.63, see table 4.3). Among the 3 CO_2-foam floods, CO2F3 resulted in the highest oil recovery 80.1% OOIP. The residual oil present after performing the water-flood is dependent on the number of snap-off events that trap crude oil and the pore body to throat ratio, i.e. pores with large bodies and narrow throats will retain more residual oil than pores

with large bodies and wider throats. During the waterflood, brine enters the smallest pores and trap the crude oil present by snap-off. CO2F3 had the lowest initial oil saturation and was presumably the stacked core system in which the fewest amount of pores were accessed during the drainage. If there is no crude oil present in the pore, no trapping can occur either. Because of the low initial oil saturation, a larger portion of the pore space may have remained 100% brine saturated, which reduces the number of snap-off events, thus leading to higher oil recovery compared to the other stacked cores.

4.3 Mobility Control

This section provides results and observations made from experiments performed on stacked cores CO2F2, CO2F3, CO2F4 and BL1. The waterflood was succeeded by either CO_2-foam flood or baseline for an additional 2.0 PV injected. Stacked cores CO2F2, CO2F3, CO2F4 and BL1 show that the initial part of the co-injection was an extension of the waterflood before additional oil was produced and this will be further discussed in the next segment. Additional oil recovery by mobility control CO_2-foam ranged between 15.7% and 22.2% OOIP, yielding a total recovery ranging from 69.3% to 80.1% OOIP for the respective stacked core systems. The baseline, BL1, recovered 29.8% OOIP during the co-injection and resulted in a total oil recovery of 87.0% OOIP. Figures 4.3-4.6 shows oil recovery versus PV injected for stacked cores CO2F2, CO2F3, CO2F4 and BL1. The blue and green points are the laboratory measured points for oil recovery from the waterflood and co-injection, respectively. Error bars of fixed value was set to 5% of calculated OOIP and included uncertainties related to pump injection rate, graded cylinder deviation and graded cylinder production reading (cf. Appendix III).

All stacked cores showed one particular similarity. The initial part of all co-injections conducted, whether surfactant was added to the liquid solution or not, appears as an extension of respective waterflood performed. The first measured point during the co-injection on figures 4.3-4.6 represents the first measured volume of crude oil recorded after the co-injected fluids has reached the core inside the Hassler core holder, i.e. dead-volume of tubing lines and valves are removed. It is suggested that a sufficient volume of injected supercritical state CO_2 is required before significant residual oil saturations are mobilized and that the oil displacement process observed while gas saturation increases is caused by the fluid travel/core length. As the gas-liquid co-injection reaches the inlet of the core, produced fluids at the outlet of the core will only consist of crude oil and brine, because the gas saturation is zero. The gas-liquid front separates two entirely different systems, where two fluids (oil and water) is ahead of the front, whereas three fluids (gas, oil and water) co-exist behind the front. The initial part of the co-injection follows the increment of the waterflood for approximately 0.3 PV.

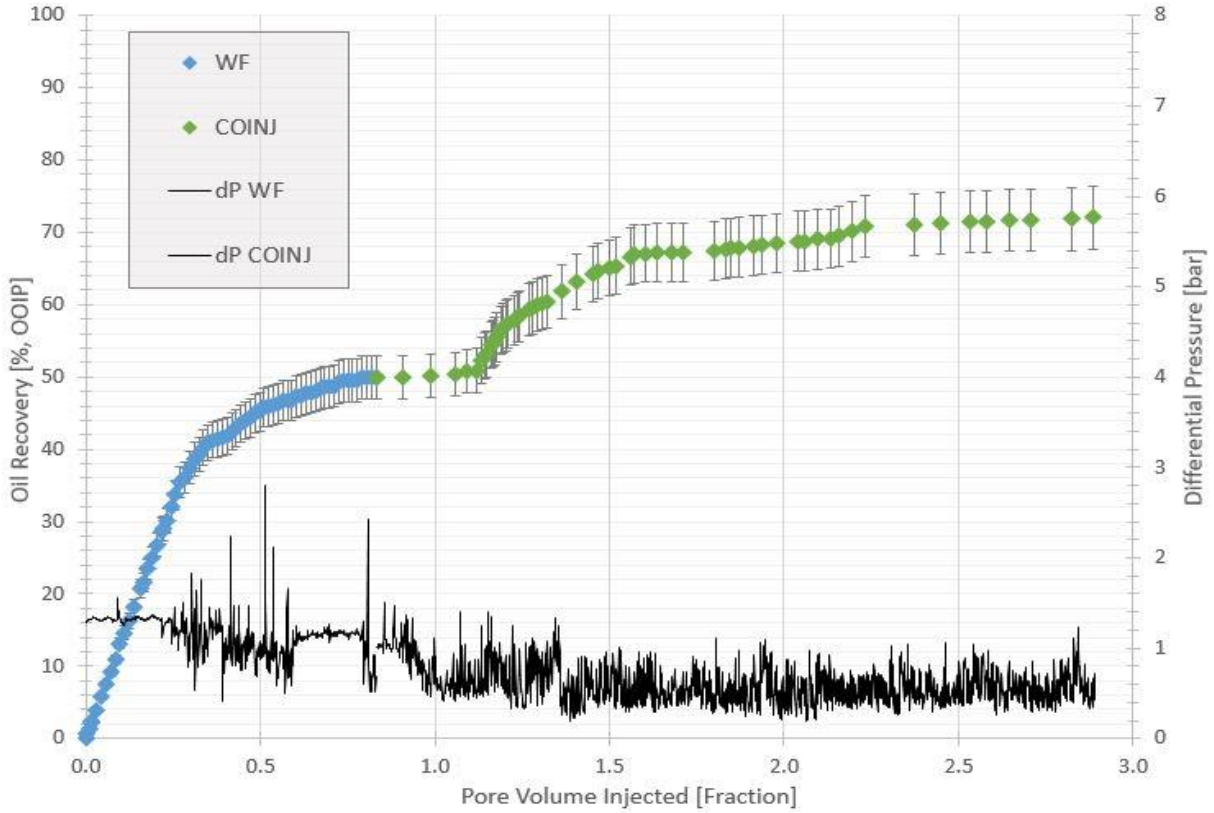

Figure 4.3: Oil recovery versus PV injected for stacked core CO2F2. Total oil recovery for this experiment was 72.1% OOIP. Water breakthrough occurred at 0.28 PV injected and a noticeable increase in oil recovery is observed at 1.12 PV during the CO_2-foam flood. Differential pressure is shown in black and included as a secondary function.

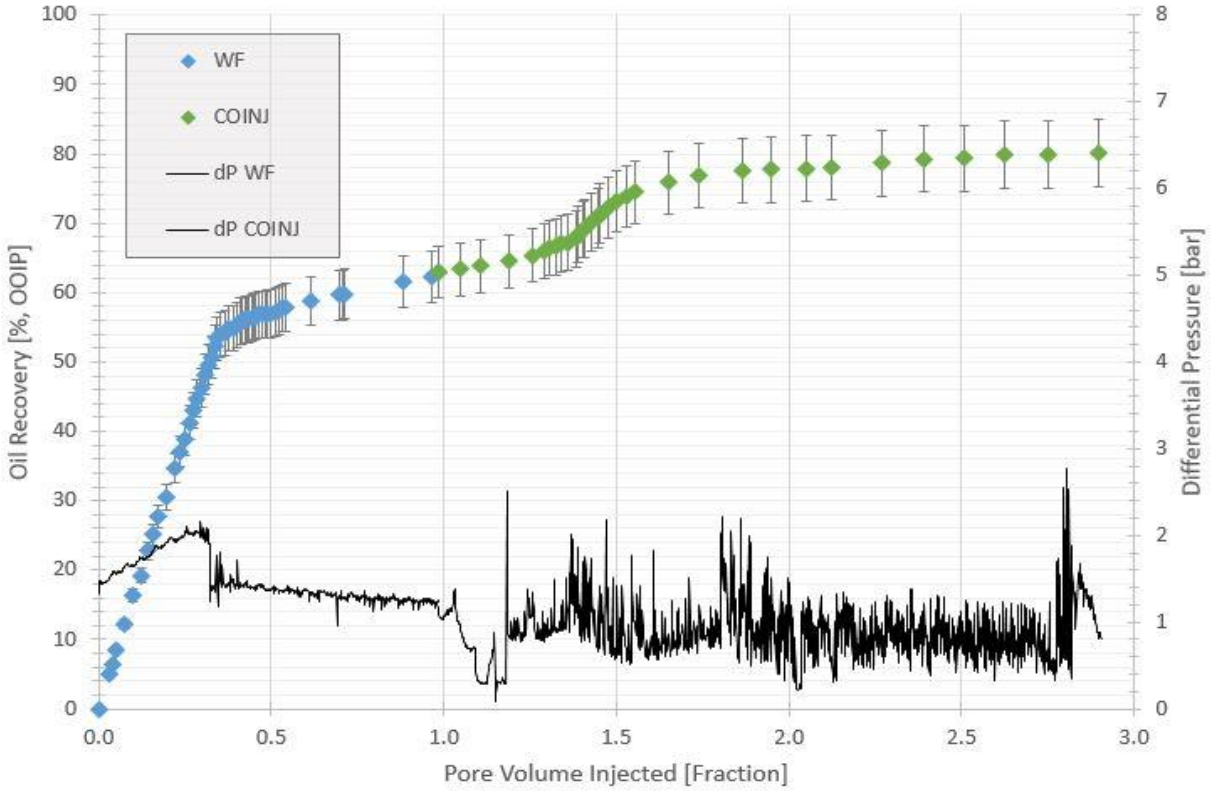

Figure 4.4: Oil recovery versus PV injected for stacked core CO2F3. Total oil recovery for this experiment was 80.1% OOIP. Water breakthrough occurred at 0.35 PV injected and a noticeable increase in oil-recovery is observed during the CO_2-foam flood at approximately 1.23 PV injected. Differential pressure is shown in black and included as a secondary function.

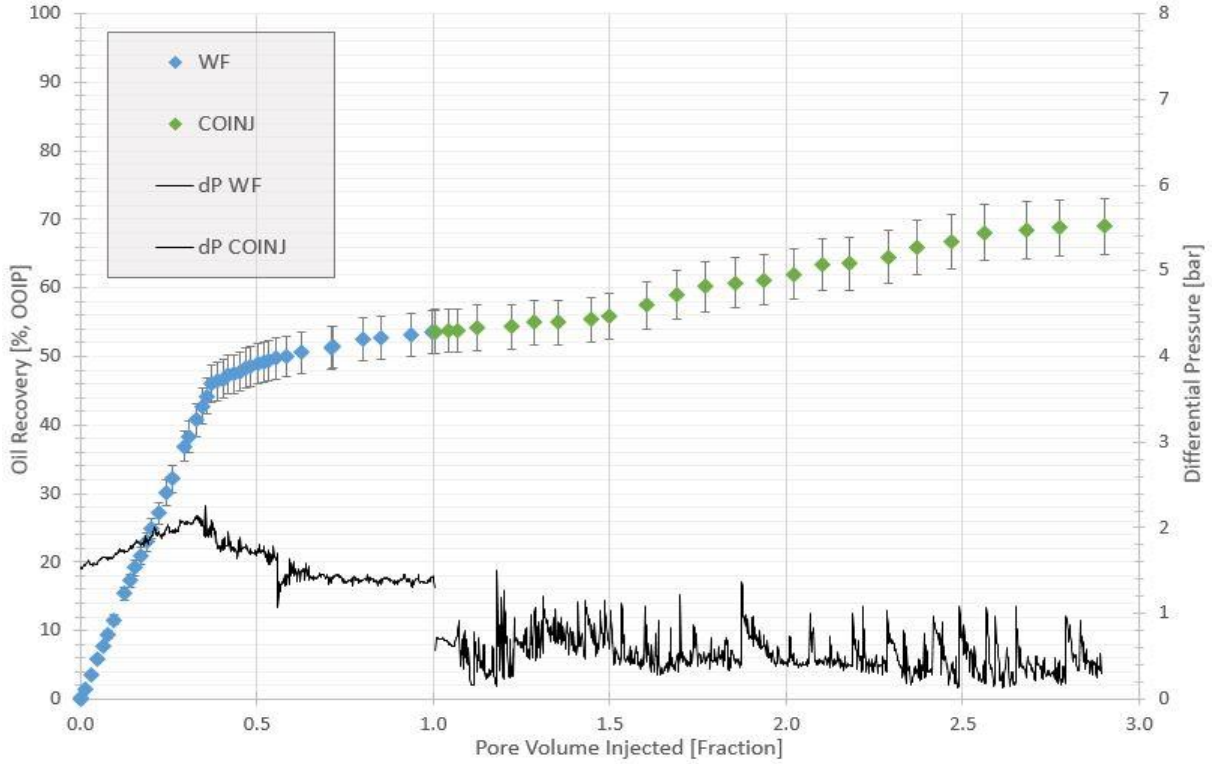

Figure 4.5: Oil recovery versus PV injected for stacked core CO2F4. Total oil recovery was 69.3% OOIP. Water breakthrough occurred at 0.36 PV injected. The CO_2-foam flood conducted in CO2F4 yield a gradual increment in oil recovery, which is opposite of what was observed in the other experiments. Differential pressure is included as a secondary function.

4.3.1 Foam Stability

Thermal degradation of surfactant affects the stability of the generated foam and may compromise the purpose of the mobility control. Based on the pressure differential observed during the CO_2-foam floods, it is not certain that the foam generated was stable, if generated at all. The average pressure differential is evidently lower than the waterflood for all CO_2-foam floods performed and the fluctuating differential pressure may derive from gas and liquid being co-injected. For the CO_2-foam mobility control investigations conducted in this thesis, there is reason to suggest that the CO_2-foam generated may have been unstable, due to thermal decomposition of surfactant.

A study at Rice University on CO_2-foam and adsorption with non-ionic surfactant show that thermal decomposition of surfactant is severe at temperatures ranging between 43°C and 80°C (Note that 43°C is the actual reservoir temperature at the field pilot held at East-Seminole, Texas). However, the same study show that surfactant decomposition was completely inhibited by adding a Na_2SO_4-component to the ES-brine at both mentioned temperatures (Jian et al., 2015). This may compromise the stability of the CO_2-foam floods performed in this thesis because the liquid solution used to generate the CO_2-foam did not contain the sodium sulfate component. The constituents of the liquid surfactant solution are a non-ionic surfactant provided by Huntsman Corporation formed with linear alcohol ethoxylates and ES-brine, where the Na_2SO_4 is excluded due to precipitation of gypsum ($CaSO_4$) when in contact with carbonate rock formations. This is confirmed by personal conversations with PhDs Marianne Steinsbø and Bergit Brattekås, whom conducted laboratory studies of ES-brine floods (Na_2SO_4 included) in Edwards Limestone. As mentioned in Section 2.2.3, because temperature in most scenarios is an unalterable parameter, thorough screening of liquid surfactant solution with the correct composition is necessary to ensure foam stability at elevated temperatures (Enick and Olsen, 2012).

4.3.2 Oil Recovery by Mobility Control

The residual oil saturation after waterflood is coherent with the balance between capillary and viscous forces present. Capillary forces snaps off droplets of oil centered in each pore that originally contained an initial oil saturation, whereas the viscous forces act against these forces by applied fluid viscosity and pressure gradient. The viscous to capillary ratio, given by the dimensionless capillary number N_{VC} (equation 2.1), determines the residual oil saturation achieved. The waterfloods performed individually on each stacked core system yield an oil recovery ranging between 49.9% and 62.9%. It is evident that the high residual oil saturations present after waterflooding is due to a low capillary number, where effects of capillary trapping of oil via snap-off surpasses the applied viscous forces.

To counter the low capillary number, supercritical CO_2 and liquid surfactant solution is co-injected to generate foam and reduce the mobility by increasing the apparent viscosity of the gas. The effectiveness of the CO_2-foam floods is coherent with the CO_2-mobility control occurring within the stacked cores. CO_2-foam flooding was, to a certain extent, successfully performed and an increase in oil recovery after the waterflood is observed for CO2F2, CO2F3 and CO2F4. As previously discussed, it is not confirmed that co-injection of supercritical CO_2 and surfactant solution generated foam in these stacked cores. However, frequently fluctuating differential pressure was observed during the co-injections, especially in stacked cores CO2F2 and CO2F3, and it is suggested that it may be ascribed to foam generation. However, all CO_2-foam floods showed a relatively low average differential pressure (ranging from 0.53 to 0.88 bar), which is believed to be a consequence of too low total injection rate. 10 ml/h was used as total injection rate in all experiments, which only amounts to 2.0 PV/day. As mentioned in section 2.2.1, leave-behind is the dominant foaming mechanism if the injection velocity is kept low, creating lamellae parallel to the gas-flow (Tanzil et al., 2002). The low average differential pressure observed may suggest that only weak foam was generated.

Irrespective of whether the CO_2-foam generated during the co-injections was weak, unstable or not generated, mobility control of the injected CO_2 has still occurred by the simultaneous injections of both gas and liquid. Although, this was not considered a WAG injection, it may show similarities in the sense that small slugs of supercritical CO_2 and liquid solution succeeds one another to maintain a stable displacement front (Enick and Olsen, 2012). Literature show that recovery efficiency from such mobility control is dependent and very sensitive to the liquid-to-gas injection ratio, because of its ability to stabilize the displacement front (Al-Shuraiqi et al., 2003). However, to maintain a stable front it is required that the liquid and gas injection ratio are optimized. An above-optimum injection ratio (more liquid and less gas than optimal ratio) is preferred because it tend to maintain stability, compared to below-optimum ratio (less liquid, more gas than optimal ratio), which promotes viscous instability and consequently enhances viscous fingering and gas-channeling (Rogers and Grigg, 2001).

In CO2F2 and CO2F3, a sharp response in oil recovery was observed during the CO_2-foam floods. The fluctuating differential pressure may derive from mobility control by either CO_2-foam generation or liquid-gas co-injection. In CO2F4, a less fluctuating differential pressure was observed, indicating that CO_2 mobility control was diminished. During this experiment, gas injection rate was increased to 9 ml/h and liquid injection rate was reduced to 1 ml/h and this may clarify why CO2F4 does not show the sharp increase in oil recovery that was observed in CO2F2 and CO2F3. The reduction of liquid solution injection rate promotes viscous instability and also reduces the total volume of surfactant eligible to generate foam. CO2F4 showed more of a gradual increment, compared to the other CO_2-foam floods

and it is presumably due to the altered liquid-to-gas ratio. The co-injection in stacked core CO2F4 was conducted to quantify the importance of correct foam quality (cf. Section 2.2.3).

4.3.3 Oil Recovery by CO_2 Dissolution

In this section, recovery by miscibility is discussed. I urge the reader to visit Appendix II – Miscibility. Several factors affect the residual oil saturation after flooding the stacked cores. It is suggested that viscosity reduction and swelling of crude oil caused by interaction with supercritical state CO_2 contribute to additional oil recovery compared with the waterflood. As the supercritical CO_2 dissolves in the crude oil, the viscosity of the oil is reduced, which increases fluid mobility (Moortgat et al., 2013). The degree of viscosity reduction is dependent on the initial viscosity of the oil, i.e. greater reduction for higher viscous oil. Crude oil specifics are listed in Section 3.2. Depending on the system pressure, the dissolution process with supercritical state CO_2 in contact with oil may cause crude oil swelling. Swollen droplets of oil force fluids that originally were immobile under experimental pressure conditions out of the pores and to the production. The increase of oil swelling increases the oil saturation in the pore space and subsequently increases the oil-relative permeability (Sasaki et al., 2013). The relative permeability of oil is presumably higher during the CO_2-foam floods compared to their respective waterflood. Crude oil and supercritical state CO_2 mixing by diffusion was also suggested to occur at this low injection rate. It is reported in literature that the effect of CO_2 dissolution and diffusivity is more pronounced at elevated temperature and pressure, enhancing mass transfer between the injected CO_2 and the present crude oil, which may improve the oil recovery (Kavousi et al., 2014). The effects of CO_2 dissolution and diffusivity has not been quantified in the experimental work done in this thesis. It is reported that residual oil saturations may evaporate when exposed to sufficient volumes of dense CO_2, which consequently questions the relevancy of the concept of residual oil saturations when conducting CO_2 injections at miscible conditions (Moortgat et al., 2013).

4.3.4 Oil Recovery by Vertical Injection

The vertical top-to-bottom injection of CO_2-foam was considered to be one of the important factors contributing to the gas mobility control. In all co-injections, the mobility control was assumed improved by vertically co-injecting the CO_2 at low injection rates. Oftentimes, segregation effects are considered a problem when injecting horizontally, because of the much lower density of the injected gas compared to the oil. The density differences causes segregation between the gas and the oil, which forces the less dense gas to rise above the oil, thus decreasing the macroscopic sweep efficiency. Because the co-injections performed in this thesis were injected vertically, this effect becomes an advantage, because the segregation contributes to maintain a stable displacement front, which is important for the sweep profile. Furthermore, the injection rates of the co-injection was also likely to contribute to maintaining a stable front by keeping viscous fingering to a minimum. Viscous fingering is caused by extreme differences in mobility between gas and oil. At ambient conditions, viscosity differences between gas and oil are in the order of several magnitudes. The velocity of the injected gas is the critical factor determining the extent of viscous fingering in a gas-oil displacement and the low injection rates used in the experiments were assumed to mitigate the effects of viscous fingering. For all stacked cores, a total injection rate of 10 ml/h was used which adds up to approximately 2.0 PV injected per day. The individual injection rates for gas and liquid during the co-injections was 8 ml/h and 2 ml/h, respectively, with the exception of CO2F4, where the CO_2-foam flood was conducted using 9 ml/h for the gas and 1 ml/h for the liquid solution.

4.3.5 Baseline Test

To quantify the effect of co-injecting liquid surfactant solution with CO_2 to generate foam, a baseline test was conducted. The baseline test serves as a comparison model for the CO_2-foam floods without having surfactant dissolved in the liquid solution. In stacked core BL1, the waterflood was performed exactly the same way as the other stacked cores and show a similar outcome in terms of water breakthrough and oil recovered. Figure 4.5 show oil recovery versus pore volumes injected for the waterflood and the co-injection. Additional oil recovery by co-injection was 29.8% OOIP and the total oil recovery was 87.0% OOIP, the highest recorded oil recovery of any stacked core system.

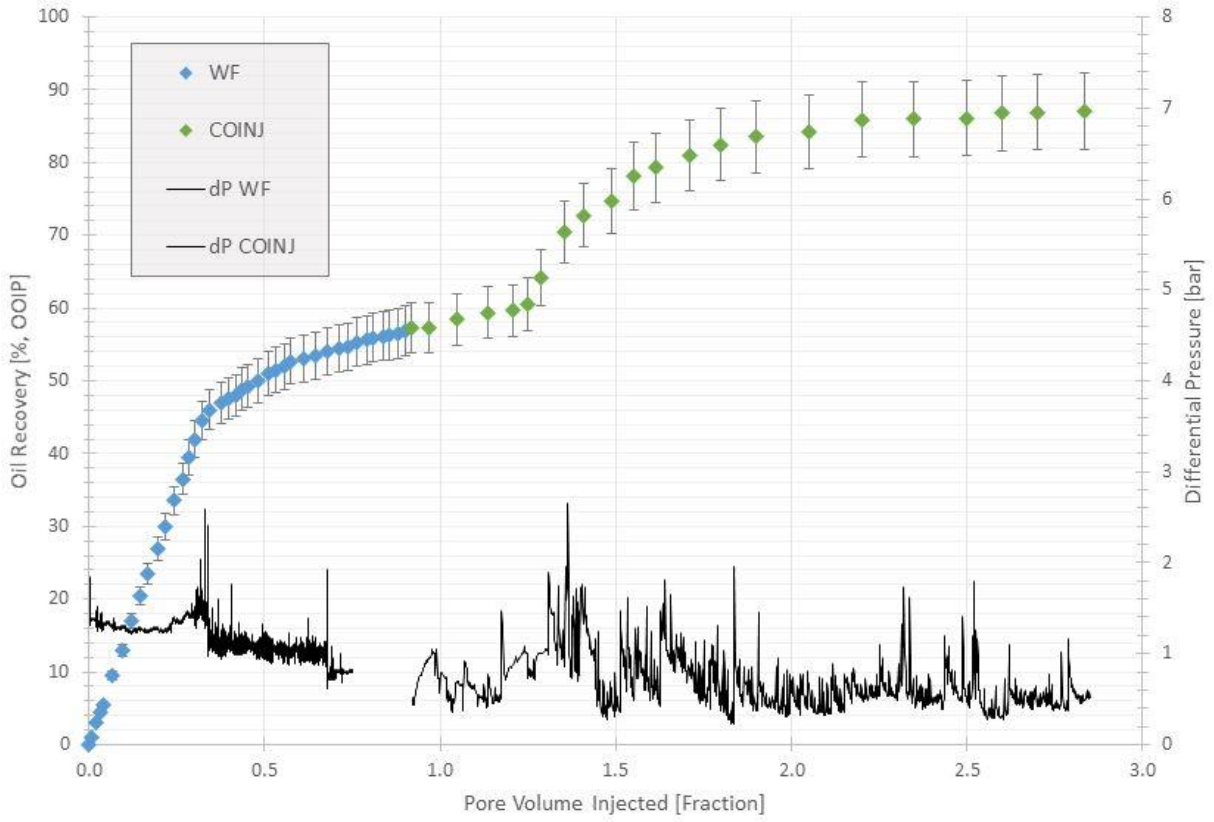

Figure 4.6: Oil recovery as function of pore volume injected for stacked core BL1. A noticeable increase in oil recovery was observed at approximately 1.25 PV injected during the co-injection. An issue with the logging tool is the reason why no differential pressure is shown between 0.75 and 0.92 PV injected during the waterflood.

The initial expectation for the baseline was that the waterflood would yield similar outcome and that the co-injection would yield a reduced additional oil recovery because of diminished CO_2 mobility control compared with the other stacked cores. Interestingly, this was not the case, as the baseline co-injection was observed to yield the highest recorded additional recovery (29.8% OOIP) and overall oil recovery (87.0% OOIP). The following segments presents observations made during the baseline test.

The waterflood conducted showed similarities in terms of water breakthrough and oil recovered. Water breakthrough occurred at 0.33 PV injected and the waterflood lasted for 0.92 PV injected, reaching an oil recovery of 57.2% OOIP. The co-injection was conducted as described in section 3.4.5 and lasted until 2.84 PV was injected. BL1 has one characteristic difference compared to the other stacked cores and that is the permeability. The absolute permeability in BL1 was measured to 45.49 mD, compared to an average of 26.81 mD ± 1.79 mD for stacked cores CO2F2, CO2F3 and CO2F4.

The improved absolute permeability in BL1 is arguably the reason why elevated oil recovery was observed during the co-injection. Initial expectations aside, it was expected that the baseline co-injection of supercritical CO_2 and ES-brine would mobilize residual oil, because it still appears as a liquid-gas co-injection. In this experiment, the only element altered compared to the other co-injections was the liquid solution, where the foaming agent was removed. This, however, does not prevent effects of CO_2 dissolution, vertical injection and mobility control by liquid-gas co-injection to influence the displacement of crude oil. It is suggested that BL1 experienced the same effects of oil-viscosity reduction, oil-mobility improvement and oil swelling by CO_2 dissolution, as well as the front-stabilizing effects of vertical injection and mobility control by liquid-gas co-injection, as was present in the other stacked cores CO2F2, CO2F3 and CO2F4. These effects contribute to increased oil recovery and may have been enhanced as a function of improved connectivity. If CO2F2, CO2F3 and CO2F4 did not generate CO_2-foam, because of thermal degradation of surfactant, it is reasonable to assume that all four (including BL1) essentially became identical experiments. The improved absolute permeability in BL1 is suggested to improve the efficiency of the co-injection, yielding an increased oil recovery compared with the other stacked cores. However, no evidence exist to confirm this suggestion.

4.4 Numerical Simulation

The initial data file made for the simulation studies done in this thesis was based on liquid production and recovery observed in the baseline co-injection of CO_2 and ES-brine, BL1. Based on skill level and knowledge working with the Eclipse engine, it was considered wise to start out with a simulation consisting of two-phase co-injection and not CO_2-foam. The first objective was to history match the waterflood, which was necessary and important. The efficiency of the displacement and fluid behavior during the simulated co-injection depends on the outcome of the previously performed waterflood. The history match between simulated waterflood and the laboratory waterflood was therefore thoroughly executed, to ensure that the model could be applicable to the other stacked core system.

4.4.1 Simulated Waterflood

The first step of the simulated waterflood was to import core-specific data. Table 4.4 show imported values, under what keyword it was specified and in which section the input data was imported.

Table 4.4: Input data, associated keyword and designated section.

Input data	Value	Keyword	Section
BL1: Core IDs	13 – 16 – 14 – 15	TITLE	RUNSPEC
Time of start	11 FEB 2016 09:20:00	START	RUNSPEC
Porosity	0.26 – 0.27 – 0.26 – 0.25	PORO	GRID
Permeability [mD]	64.5 – 62.3 – 53.5 – 47.4	PERMZ	GRID
Density Water (SC)	1020.3	DENSITY	PROPS
Density Oil (SC)	875.3	DENSITY	PROPS
Experimental Pressure [bar]	84.42	PRESSURE	SOLUTION
Initial Water Saturation	0.29 – 0.29 – 0.29 – 0.29	SWAT	SOLUTION
Well Specifics	WINJ / PROD	WELLSPEC	SCHEDULE
Grid Cell Completion	1-1-1 / 1-1-400 (x, y, z)	COMPDAT	SCHEDULE

In Table 4.4, the absolute permeability is specified by the PERMZ keyword. The waterfloods and co-injections performed during the experimental work was injected vertically, top-to-bottom, and the PERMZ keyword specifies the permeability values in *Z* (vertical) direction. PVT and SCAL properties such as water-oil relative permeability table and oil PVT properties are included in PROPS section.

To observe results after simulating, the E100 engine requires that several output requests are specified in the SUMMARY section. The following output data were requested in each simulation run:

- WWIR – Well Water Injection Rate
- WWPR – Well Water Production Rate
- WOPR – Well Oil Production Rate
- WBHP – Well Bottom Hole Pressure

After building an initial BASE_SIM data file including all necessary parameters, the simulation process was ready to be initiated. A test-run was performed to evaluate performance of the BASE_SIM data file and preliminary results were obtained. The BASE_SIM data file served as a foundation for adjustments and tuning, that eventually would end up as a base model for the simulated waterflood.

The results obtained in each simulation run were imported in Petrel to enable visualization of the simulated data and interpretation of the output requests that were specified in the SUMMARY. All results were plotted as liquid production rate (Sm^3/day) versus time step and bottom hole pressure versus time step. Figure 4.7 illustrates the results obtained from running the initial BASE_SIM data file. To be able to evaluate the performance of the simulation, observed laboratory data was imported.

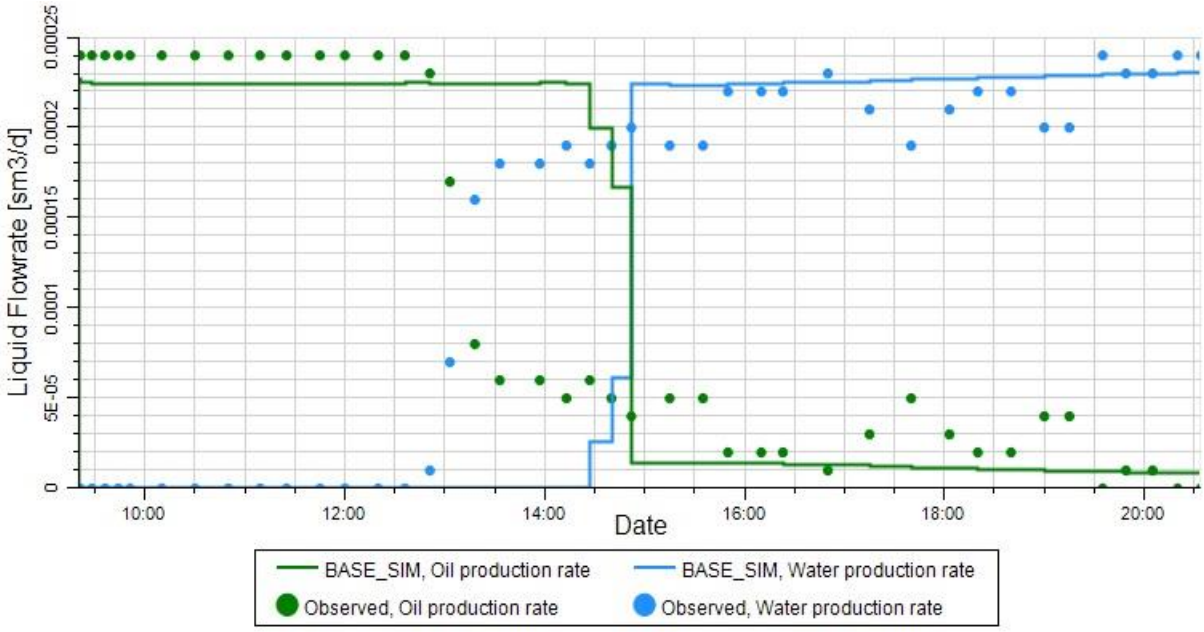

Figure 4.7: Liquid flowrate plotted versus time. Solid lines are simulated liquid production and the dots are *global observed data*, i.e. recorded liquid production data from the laboratory, which was imported in Petrel as an input file.

The performance of the simulation was dependent on the concurrence with the observed laboratory data and as observed in Figure 4.7, simulated liquid production did not coincide with the observed laboratory data. Water breakthrough in the simulation occurred much later than the laboratory waterflood and it was suggested that the late breakthrough of water was caused by water movement being impaired by low water-relative permeability in the low-to-mid water saturation interval.

Unfortunately, no relative permeability measurement was conducted on the core plugs and the stacked core systems during the laboratory work. Instead, relative permeability values for oil and water was obtained from experimental and simulated work done by (Hamon, 2004). Before altering the relative permeability, several other attempts to enable earlier movement of water were attempted. First, the initial water saturations in each of the four cores were altered while still honoring the average of the stacked system, which was measured after conducting primary drainage and 0.29 for BL1. The first core in the stacked system was assigned to have a slightly decreased value, which was increased in succeeding order down the stacked core. The input data specified under the SWAT keyword was 100*0.25 100*0.27 100*0.31 100*0.33. This input line reports to the simulator that the first 100 cells is specified with an initial water saturation of 0.25 and that the 100 next cells has 0.27 and so on. The alteration of initial water saturation did not improve movement of water. However, specifying individual initial water saturations for each core is likely to be more realistic than assuming an average for the whole system. The next attempt was to introduce the SWCR keyword in the PROPS section, which is Scaled Critical Water Saturations and defines the largest water saturation at which the water relative permeability is zero. However, this attempted adjustment failed as well and did not result in any improvement related to earlier breakthrough or better concurrence with the observed data.

The next step was to adjust the relative permeability values of oil and water to improve water movement at an earlier stage of water saturation, while still honoring the overall assumption that all stacked cores exhibited strongly water-wet characteristics. Methodically this was done by keeping one parameter, either relative permeability of water or oil, constant while adjusting the other. During this sensitivity study, adjustments to increase or reduce relative permeability, promote earlier crossover and increase or reduce end-points were tested. The performance of the sensitivity study was evaluated by how it improved the concurrence with observed liquid production data and the best resulting data file was saved. Figure 4.8 schematically illustrates the original oil-water relative permeability values (BASE_SIM) and the new values obtained after conducting the sensitivity study (BL1_SIM). Figure 4.9 illustrates the adjusted liquid production rate versus time step after altering the relative permeability.

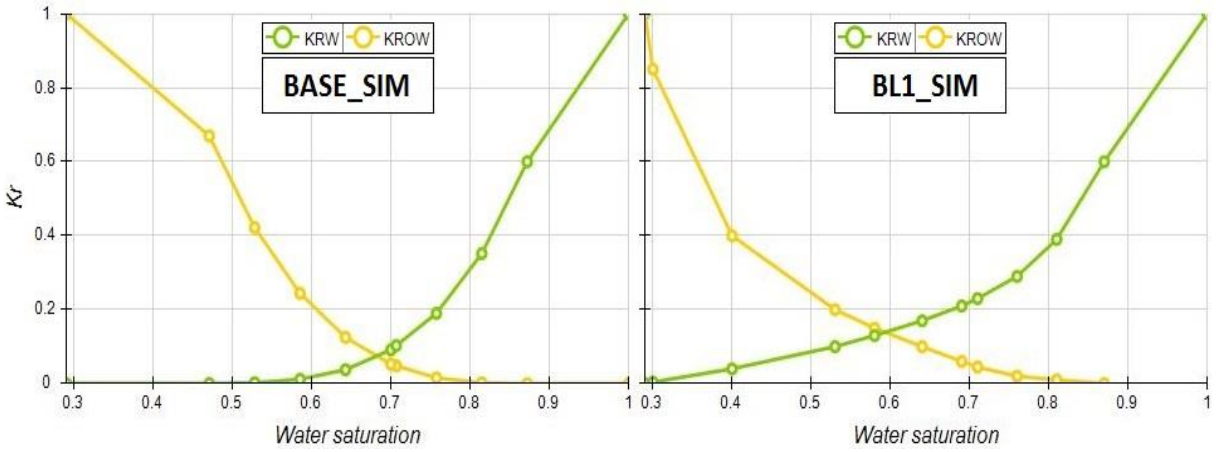

Figure 4.8: Left chart illustrates the relative permeability curves for oil and water obtained from (Hamon, 2004). The right chart show the new relative permeability curves that was empirically evaluated to best match the global observed data.

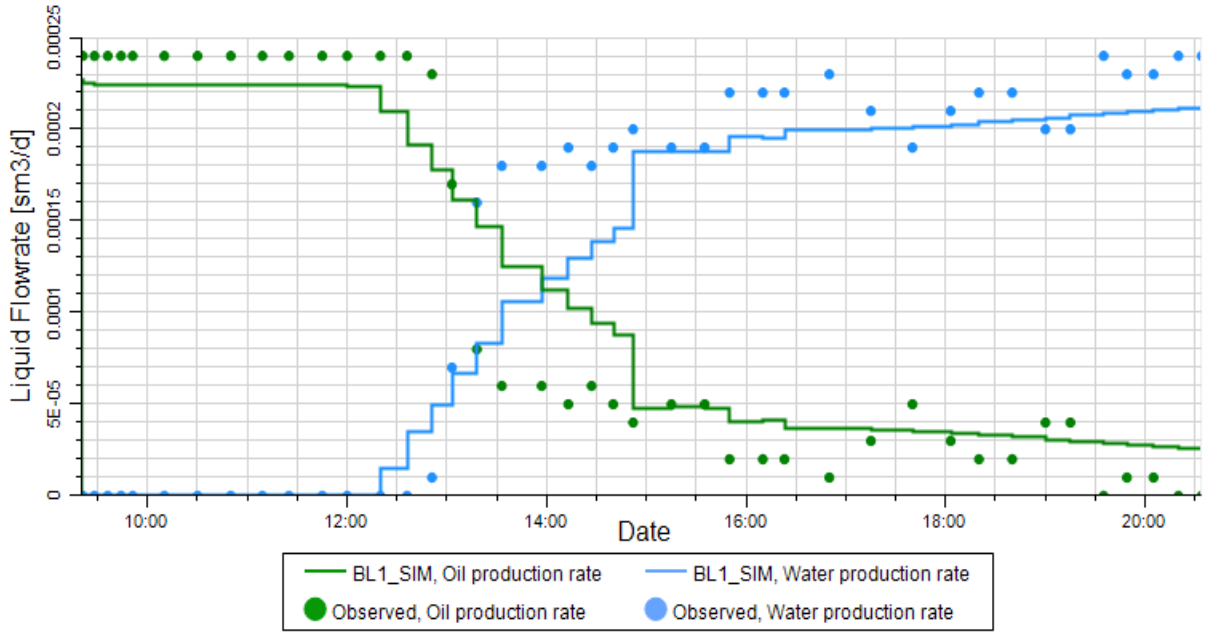

Figure 4.9: Liquid flowrate plotted versus time for both simulated data (lines) and global observed data (dots). The liquid production recorded after adjusting the water-relative permeability to enable water movement earlier resulted in water breakthrough at approximately the same time as observed during the laboratory experiment. The increment of the first water production is slightly off but the overall show a much better concurrence with observed data, compared with BASE_SIM, Figure 4.7. The simulated oil and water production rates is observed to follow each other in opposite directions.

During the simulation process, the BHP was monitored and was observed to coincide with the observed pressure logged with the pressure transducers during the laboratory waterflood. Figure 4.10 show inlet pressure and outlet pressure versus time steps for simulated and observed pressure. The simulated pressure matches the observed pressure and a response is observed during two-phase production.

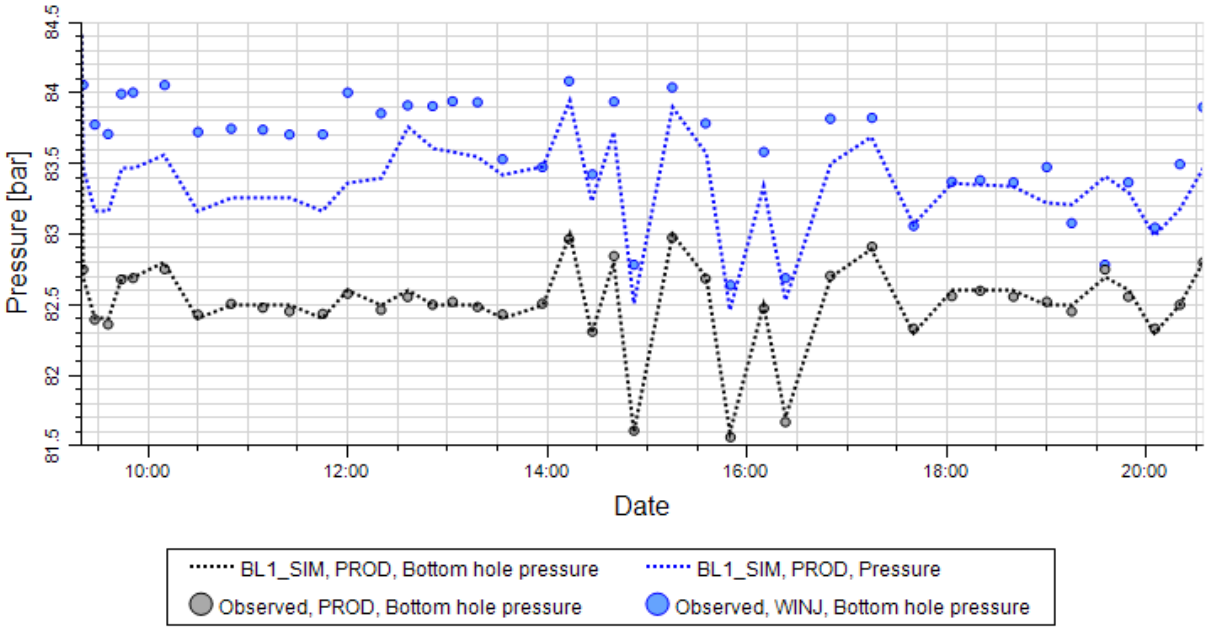

Figure 4.10: Inlet and outlet pressure versus time for simulated data (dotted lines) and global observed data (dots). Blue color represents observed and simulated pressure data at the inlet side, whereas black represents the outlet data.

Figures 4.9 and 4.10 show that the simulated data represent a good reproduction of the experimental waterflood. Even though the simulated waterflood did not yield absolute concurrence with the observed laboratory data, the history match was considered satisfactory. The simulation data file, BL1_SIM.DATA, and sections PROPS.INC, SUMMARY.INC and SCHEDULE.INC are found in Appendix V.

4.4.2 Simulated Co-injection

After initiating the simulated co-injection a few, but quite important deficiencies surfaced. 1) No gas production was recorded during the experimental work. The simulator is, as mentioned in Section 3.5, calculating mass-balance at each defined time step. Because only liquid production (brine and crude oil) was measured at the laboratory, the simulated production becomes uncertain due to CO_2 production not being defined by observed data. 2) Three-phase relative permeability was not measured and the generic input data generic is associated with uncertainty. It was observed that the mass-balance was heavily influenced by the relative permeability, thus a representative three-phase relative permeability measurement is necessary to enable satisfactory history matching. The simulated co-injection in BL1 performed in this thesis was thus considered to be an unsatisfactory representation of the experimental work. In addition to mentioned arguments, the E100 black oil simulator assumes that all compositions remains unchanged throughout the simulation, i.e. no gas-oil miscibility. Even though the extent of gas-oil miscibility in terms of gas dissolution, crude oil evaporation and diffusivity, was not quantified in the range of this experimental work, it is suggested that a compositional fluid model that includes equations of state is necessary to capture accurate simulated fluid behavior.

5. Concluding Remarks

This chapter presents conclusions and possible future work obtained after conducting experimental study of mobility control CO_2-foam by co-injection of supercritical CO_2 and liquid surfactant solution in stacked core systems of heterogeneous Edwards Limestone.

5.1 Conclusions

- Waterflooding was successfully performed and the resulting oil recoveries ranged between 49.9% and 62.9% OOIP. Core CO2F3 showed higher oil recovery during the waterflood, which may have been caused by the primary drainage conducted on this specific stacked core system.

- Mobility control of supercritical state CO_2 was successfully conducted in three experiments (CO2F2, CO2F3 and CO2F4). The overall oil recovery in these stacked core systems ranged between 69.3% and 80.1% OOIP. Cores CO2F2 and CO2F3 showed a sharp response in incremental oil recovery after approximately 0.3 PV injected during co-injection, compared with the gradual increment of oil recovery observed in core CO2F4.

- The low differential pressure measured during co-injections in CO2F2, CO2F3 and CO2F4 suggests weak or unstable foam generation. The low total injection rates used in the experimental work and thermal decomposition of surfactant may have contributed to the lack of strong foam generation.

- It was proposed that the vertical injection, top-to-bottom, enhances the sweep efficiency for all co-injections conducted by maintaining a displacement front stabilized by the density differences between supercritical CO_2 and crude oil. The injection rates used suggests minimum viscous instability by effects of fingering and channeling.

- The baseline test, BL1, was conducted by co-injecting supercritical state CO_2 and ES-brine to evaluate and quantify the importance of foam generation for mobility control. This baseline, however, recovered the highest recorded percentage of OOIP (87.0%). It was suggested that the absolute permeability in BL1, compared to the other experiments, was caused by improved interaction between the supercritical CO_2 and the crude oil.

- A successful numerical history match of the experimental waterflood was conducted during a sensitivity analysis using a base model constructed to resemble the experimental conditions. It was shown that the history match was strongly sensitive to oil-water relative permeabilities.

5.2 Future Work

- Screening of surfactant and liquid solutions to ensure foam stability in carbonate reservoirs at elevated temperatures. Also, in-situ foam generation by single cycle SAG to evaluate the effects of pre-injecting a slug of liquid surfactant solution.

- Increase total injection rate during CO_2-foam floods above minimum required to generate foam by snap-off to evaluate the benefit of strong foam compared to weak foam.

- It was suggested that the increased oil recovery in BL1 was caused by improved absolute permeability, compared to the other stacked core systems. Quantify this influence.

- It is proposed that the additional oil recovered during liquid-gas co-injection may have been affected by the vertical top-to-bottom injection strategy, where gravity segregation and mitigated viscous instability contribute to maintain a stable displacement front. However, a more realistic scenario is horizontal injection and it would be interesting to conduct these investigations under the same experimental conditions, but in horizontal alignment.

- Determine miscibility by CO_2 dissolution and diffusivity in crude oil under similar experimental conditions, to evaluate the contribution of oil-gas mass transfer on the overall oil recovery.

- Evaluate the fluid flow in these three-phase systems by introducing imaging via MRI or PET/CT.

- In numerical simulation, build a compositional fluid model of multicomponent Ekofisk crude oil and perform a history match with the co-injections using compositional simulator E300. Obtain representative three-phase relative permeability values.

- Perform sensitivity parameter study on the grid. The grid is homogeneous because it is defined with only 1 cell in *X* and *Y* directions, which does not correctly represent the experimental heterogeneous domain. This can be achieved by introducing LGR (Local Grid Refinements).

Appendix I – Abbreviations and Nomenclature

BPR	Back Pressure Regulator
CCUS	Carbon Capture Utilization and Storage (or Sequestration)
CDC	Capillary Desaturation Curve
CGI	Continuous Gas Injection
CMC	Critical Micelle Concentration
CO_2	Carbon Dioxide
COINJ	Co-Injection
DOE	Department Of Energy
EOR	Enhanced Oil Recovery
IEA	International Energy Agency
IFT	Interfacial Tension
IPCC	International Panel on Climate Change
MMP	Minimum Miscibility Pressure
N_2	Nitrogen
NCS	Norwegian Continental Shelf
NPD	Norwegian Petroleum Department
OFE	Office of Fossil Energy (part of DOE)
OIP	Oil In Place
OOIP	Original Oil In Place
PV	Pore Volume (Injected)
PVT	Pressure/Volume/Temperature
RC	Reservoir Conditions
SAG	Surfactant Alternating Gas
SACROC	Scurry Area County Reef Operators
SC	Standard Conditions
SCAL	Special Core Analysis
VCP	Volumetric Change Parameter
WAG	Water Alternating Gas
WEC	World Energy Council
WF	Waterflood

K	Absolute Permeability
A	Area
V_b	Bulk Volume
N_{VC}	Capillary Number
u	Darcy Velocity
ρ_b	Density of Brine
ΔP	Differential Pressure
m_d	Dry Weight
k_i	Effective Permeability
Q	Flow Rate
$S_{O,IW}$	Initial Oil Saturation
σ	Interfacial Tension
L	Length
λ_i	Mobility (of phase i)
M	Mobility Ratio
S_O	Oil Saturation
V_P	Pore Volume
ϕ	Porosity
P	Pressure
k_{ri}	Relative Permeability
S_{Or}	Residual Oil Saturation
m_S	Saturated Weight
T	Temperature
μ	Viscosity
V_O	Volume of Oil
θ	Wetting Angle

Appendix II – Fundamental Parameters

This Appendix is provided as an addition to the thesis. Parameters of interest discussed in Appendix II will cover Wettability, Permeability, Interfacial Tension, Capillary Pressure, Mobility and Miscibility.

Wettability

In a scenario where two immiscible fluids co-exist in contact with a solid surface, both cohesive forces and adhesive forces are present. The cohesive force is the attraction between two molecules of same type, otherwise known as intermolecular forces. The adhesive force is the attraction between molecules of different type, such as water tending to spread out on a piece of glass. The adhesive force is of interest when discussing wettability because the fluid that has the strongest attractive force towards the surface is also the *wetting fluid* and will spread out on the surface of the rock (Lien et al., 2007). The degree of wettability is calculated by determining the *wetting angle, Θ,* between the wetting fluid and the surface of the solid. The wetting angle and the wetting characteristics related to the angle are illustrated in figure A.1.

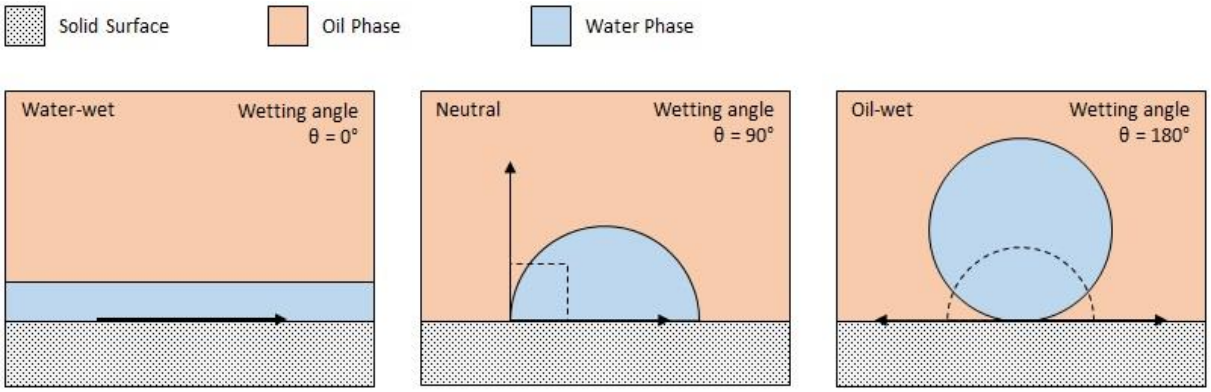

Figure A.1: Illustration of two liquid phases in contact with a solid surface. The figure show the wetting characteristics if the wetting angle is 0°, 90° and 180°. This figure is a modification of figure 5.9 of (Lien et al., 2007).

Consider a situation illustrated in figure A.1, where oil and water are present in contact with a solid surface. If the wetting angle between the solid surface and water is 0°, the wetting characteristics becomes strongly water-wet. In this case, water completely coats the solid surface, keeping the oil separated as a continuous phase through the center of the pores. A wetting angle of 0°-30° is regarded as a strongly water-wet system. The opposite case is what is illustrated on the far right, where the wetting angle is 180°. The solid surface prefers oil as the wetting phase and the adhesive force towards the surface causes the water molecules to form spherical droplets of water. It is regarded as a very oil-wet system if the wetting angle is 150°-180°. Between the two extremes there are three more characteristics, preferentially water-wet (θ = 30°-90°), preferentially oil-wet (θ = 90°-150°) and neutral wettability (θ = 90°). In the latter case, it is neither water- or oil-wet. However, in most reservoirs there is a mixed wettability due to a change wetting characteristics over time as oil migrates and settles. Mixed wettability is categorized as either MWL (Mixed-Wet Large: oil-wet in large pores), MWS (Mixed-Wet Small: oil-wet in small pores) or FW (fractional-wetted: mixed wettability in all pore sizes) (Sorbie and Dijke, 2005). The cores used in this thesis are assumed to be strongly water-wet.

Absolute, Effective and Relative Permeability

Oil, gas and water are found in varying proportions in most petroleum reservoirs, whereas permeability measurements are performed with only a single fluid present. A correction is thus necessary in order to reflect the actual permeability as a function of saturation. Each specific fluid will have an effective permeability depending on the distribution of saturation within the rock formation. Relative permeability is simply the ratio between the effective permeability of a fluid measured at a certain saturation to the absolute permeability of the rock formation (Lucia, 2007). Absolute permeability is the permeability measured with only one fluid present, commonly air or water. Relative permeability is therefore expressed as a number between 0 and 1, and as a function of fluid saturation. The effective permeability is modified from Darcy's law:

$$k_{e,i} = \frac{q_i \cdot \mu_i}{A} \frac{L}{\Delta p_i} \, , i = o, w, g \qquad \textbf{A.1}$$

$$k_{r,i} = \frac{k_{e,i}}{K} \, , i = o, w, g \qquad \textbf{A.2}$$

Above, the relationship between absolute, effective and relative permeability is described. While effective and relative permeability is dependent on type of fluid, absolute permeability is not. Absolute permeability is simply a measure of the rocks internal tortuosity. In a system where only water and oil is present at equal saturations ($S_w = S_o = 0{,}5$) and the measured relative permeability for oil, $k_{r,o}$, is 0,33 in a 60 mD rock sample, the effective permeability of the oil at 50% water saturation is said to be 20 mD. This example is a simplification of the reality where there are several factors affecting relative permeability. Fluid saturation is the most important factor, but pore geometry and distribution, wettability and fluid saturation history (e.g. Imbibition or drainage) constitutes great impact on the relative permeability of a fluid. Below, a display of typical relative permeability curves shown in two different wettability regimes, strongly water-wet and strongly oil-wet (Lucia, 2007).

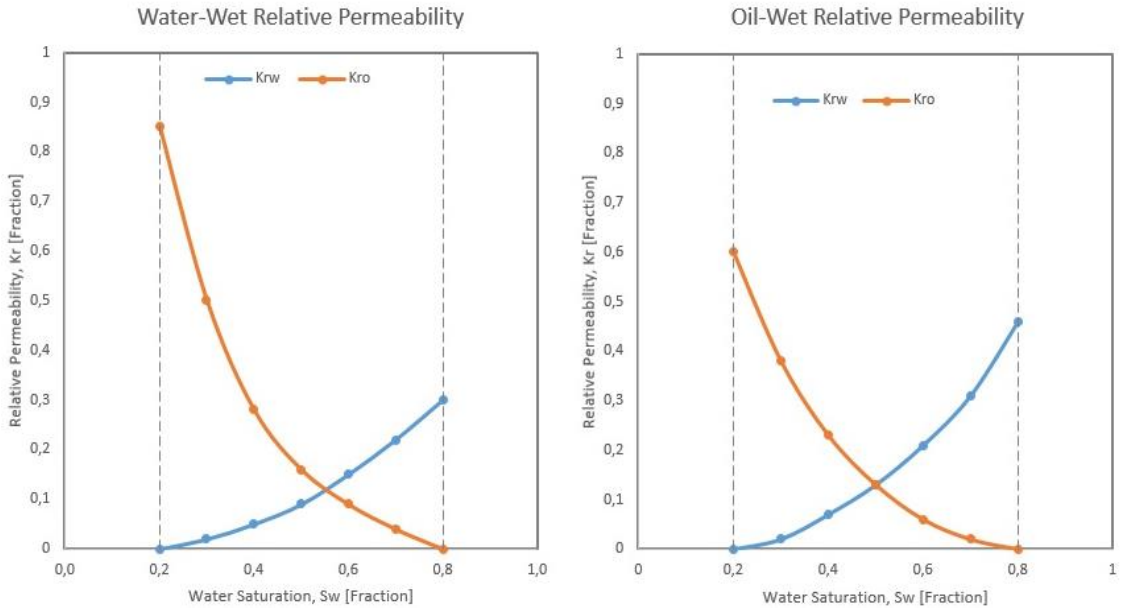

Figure A.2: Schematic diagram showing typical relative permeability curves under water-wet and oil-wet conditions. Irreducible water saturation, S_{wi} , and residual oil saturation, S_{or} , are shown as the dashed lines at $S_w = 0{,}2$ and $S_w = 0{,}8$.

Figure A.2 illustrates distinct differences in fluid flow for both oil and water between the two wettability regimes. In the water-wet regime, the relative permeability for oil is very high to begin with. The reason for that is that the irreducible water that is present is clinging to the pore-walls, leaving the oil free to move in the center of the pore. In the oil-wet regime, however, the irreducible water is now capillary bound droplets centered in the pore because oil is the preferred wetting fluid. This impairs the ability for the oil to flow as easy as in the water-wet situation. As the water saturation reaches residual oil, the situation is the same, but opposite. In the oil-wet regime, water moves freely in the center and in the water-wet regime, movement of water is limited because of oil occupying the center.

Interfacial Tension

Interfacial tension is an important parameter during foam studies because it enables gas to be mixed and stabilized as separate gas-bubbles dispersed in the liquid phase. Interfacial tension, IFT, is a measure of the energy needed to keep two fluids apart, and IFT exist in all situations where two fluids are in contact. The amount of energy is constant if temperature and pressure is held constant and is highly dependent on the composition of the two fluids. Between two fluids there are two main forces acting that decide whether the fluids will mix or not, intermolecular and intramolecular. Intermolecular is the attraction between two molecules of different fluids. Intramolecular is the attraction between two molecules of the same fluid. When two liquid phases co-exist in porous medium of heterogeneous nature, in various saturations, there may exist three possible IFTs (Zolotukhin and Ursin, 2000):

- $\sigma > 0$: The interfacial tension is positive. In this case, the intramolecular forces are stronger than the intermolecular and therefore the fluids are immiscible.
- $\sigma < 0$: The interfacial tension is negative. The intermolecular forces are stronger and the fluids will mix instantaneously.
- $\sigma = 0$: The interfacial tension is zero. The intramolecular and the intermolecular forces are equal, meaning that each molecule is equally attracted other molecules of both fluids. The fluids are miscible and the mixing process will be carried out by diffusion, as long as no outside force or disturbance is applied, until equilibrium is established.

Capillary Pressure

Capillary pressure, P_C, is the molecular pressure difference between two immiscible fluids. Whenever two immiscible fluids co-exist in a tube, a meniscus between the two fluids develops. The curvature of the meniscus is axisymmetric and dependent on the adhesive force of the wetting fluid (Zolotukhin and Ursin, 2000). Because the fluids are immiscible, interfacial tension between the two is also present. Lastly, the wetting fluid and the surface of the pipe will create an angle known as the wetting angle, Θ. Derived from the Laplace Equation, capillary pressure in a tube or pipe can be written as:

$$P_C = P_{nw} - P_w = \frac{2\sigma_{nw,w}\cos\theta}{r_C} \qquad \textbf{A.3}$$

In equation A.1, the terms P_{nw} and P_w are referred to as internal molecular pressure of the *non-wetting phase* and the *wetting phase* and the $\sigma_{nw,w}$ is the IFT at the interface separating the two fluids.

When talking non-wetting and wetting phases, it is common to regard water as the wetting fluid and oil as the non-wetting fluid. For oil to accumulate in a reservoir, the pressure in the oil phase must exceed the pressure in the water phase. If the numerator of equation A.3 is held constant, i.e. equally wetted distribution in all pores with a constant interfacial tension between the phases, the only parameter determining the capillary pressure of a pore is the pore throat radius. Thus, the largest pore throats will have the lowest capillary pressure to overcome during oil accumulation and consequently the smallest pores will have yield the highest capillary pressure.

The concept of capillary pressure is important during foam floods because foam generation by snap-off is dependent on the capillary pressure where the gas is invading. The gas invasion of a throat requires that the phase pressure exceed the capillary entry pressure of throat. As gas-pressure builds up, the curvature at the interface between the gas and the liquid increases and eventually breaks. The entry pressure at the throat is for a brief moment lower than the neighboring pressure gradient and gas invades the pore. As the entry pressure rebuilds, water drains from the pore walls in opposite direction of the gas flow and bridges the pore throat and ultimately snaps-off the gas segment into a separated gas-bubble (Rossen, 2003).

Mobility

Studying displacement of oil by gas injection heterogeneous porous medium is impossible without considering and evaluating the importance of mobility. Mobility is the ease of movement for fluids distributed in various saturations in a porous media and can be described as the relationship between the maximum relative permeability and the viscosity of a fluid (Zolotukhin and Ursin, 2000).

$$\lambda_w = \frac{K\ k_{rw,or}}{\mu_w} \qquad \textbf{A.4}$$

K is the absolute permeability defined as the ease at which it is possible for a fluid to flow through a porous medium, and measured using Darcy's Law. Equation A.4 is an example of how mobility is defined and the same equation is applied to define oil and gas mobility. $K_{rw,or}$ is the end-point relative permeability of water when the system is at a state where the other phase is immobile, in this particular case oil. μ is the fluid viscosity. The dominant factor describing fluid flow behavior during a displacement process is the mobility ratio, which is how easily one fluid flows compared to the other:

$$M_{wo} = \frac{\lambda_w}{\lambda_o} = \frac{k_{rw,or}}{k_{ro,iw}} \frac{\mu_o}{\mu_w} \qquad \textbf{A.5}$$

$$M_{go} = \frac{\lambda_g}{\lambda_o} = \frac{k_{rg,or}}{k_{ro,iw}} \frac{\mu_o}{\mu_g} \qquad \textbf{A.6}$$

Floods where the mobility is lower than or zero ($M \leq 0$) is considered efficient, because the result is a stable displacement front, giving a good macroscopic sweep efficiency. In cases of high mobility ratio ($M > 0$), e.g. and immiscible displacement of oil with gas, the displacement front is unstable and is very dominated by viscous effects such as fingering and channeling. In this situation most of the Original Oil in Place, OOIP, is bypassed, thus leading to reduced oil recovery. The primary objective of improving the mobility control is to reduce the tendency of viscous instability causing fingering and channeling.

Miscibility

It is important to distinguish between solubility and miscibility when discussing the topic of mixing substances. Solubility is the general ability of one limited amount of one substance to mix with another to form a single homogenous phase, called a solution. Miscibility, on the other hand, is defined as the physical condition allowing two or more substances to mix in all proportions without the occurrence of an interface, to form a single homogeneous phase (Holm, 1986).

When producing oil by injection of water the process is immiscible because water is not soluble in oil. In this system, the co-existence of water and oil in the porous media leads to trapping by snap-off and a large residual oil saturation. However, if we consider the situation where the displaced phase and the displacing phase is miscible, e.g. CO_2/HC-gas displacing oil, the process becomes a miscible displacement. A miscible displacement is the displacement of a fluid that has no interfacial tension (IFT = 0) with the displacing fluid, which will lead to zero residual oil in all regions swept (Holm, 1986).

To help explain the processes of miscible displacement it is common to use ternary diagrams. Figure A.3 illustrates the first-contact and multiple-contact miscibility processes through a ternary diagram with corners representing compositions of the injected gas. The diagram also show a two-phase region enclosed by the bubble-point and the dew-point line and the critical tie line (blue dashed line).

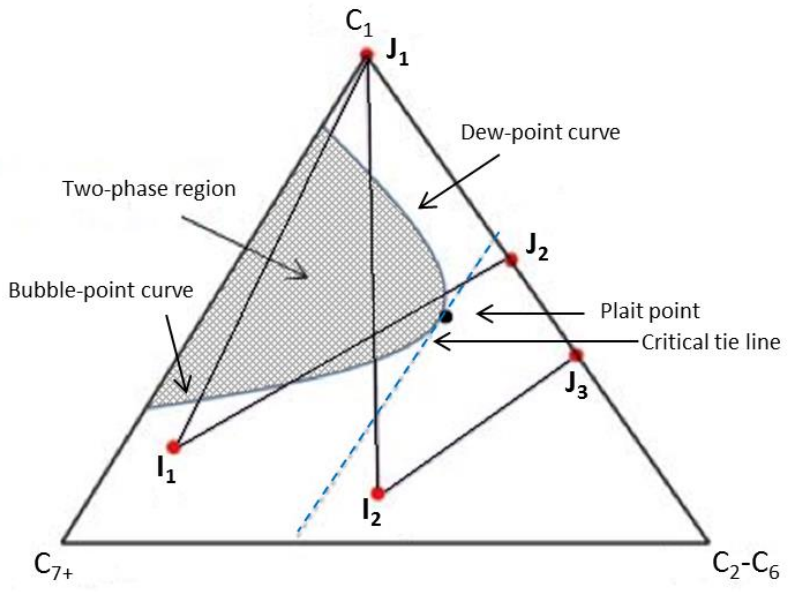

Figure A.3: Ternary diagram showing the dilution paths of the different miscible processes. *I* represent the reservoir oil composition. *J* represent the injected gas composition. The line connecting the two is called a dilution path. In this figure dilution paths for first contact (I2-J3), Condensing Gas drive (I2-J1) and Vaporizing Gas Drive (I1-J2) miscibility is shown. Immiscible displacement (I1-J1) is also included. Modified from (Skarestad and Skauge, 2012).

In general, there are two types of miscible processes depending on the composition of the fluids: *First-contact* miscible displacement and *multiple-contact* miscible displacement. Gas displacement by multiple-contact miscible processes can be developed by two mechanisms: *Vaporizing Gas Drive* and *Condensing Gas Drive*. The experimental work done in this thesis includes supercritical CO_2 and multicomponent crude oil and it is suggested that miscibility via multiple-contact is dominating.

First-contact

A displacement process where any amount of solvent injected still exists in one single hydrocarbon phase is called a first-contact miscible displacement. This process is the most direct method to achieve miscibility and the solvent mixes completely with the oil in place. To create a first-contact miscible process in a reservoir where CO_2 is chosen as solvent, a fully miscible slug must be injected ahead of the CO_2. This slug can be a lighter hydrocarbon component such as propane. The important property of the slug is that it has to be completely miscible with both the oil at the leading edge and solvent on the tailing edge. The sweep will continue as long as the slug is not bypassed or insufficient amount of slug material has been injected (Mathiassen, 2003). In Figure A.3, the dilution path between I2 and J3 represents the process of first-contact miscibility. The dilution path does not intersect the two-phase region and the displacement will consist of one single hydrocarbon phase.

Multiple-contact

In multiple-contact miscible processes, the injected gas phase condenses into the oil phase or vaporizes lighter oil components. Both processes can occur individually or in combination. Derived by its name, mass transfer by multiple-contact miscibility is achieved when the injected gas and the reservoir oil come in contact at multiple occasions. The two main mechanisms forcing multiple-contact miscibility is referred to as Condensing Gas Drive and Vaporizing Gas Drive. In vaporizing gas drive (I1-J2, Figure A.3), injected lean gas (usually C_1 or other low molecular-weight gases such as nitrogen or CO_2) vaporizes the intermediate components (C_2-C_6) from the crude oil at the interface between the phases and miscibility will develop as long as the critical tie line separates the gas and the crude oil. Injected CO_2 offer an advantage during such a displacement because of its ability to extract some of the heavier components (C_{7+}) of the crude oil (Holm, 1986, Lake, 1989). In gas condensation (I2-J1), enriched gas that contains intermediate components (C_2-C_6) condenses out of the gas phase and into the reservoir oil. After condensation, the injected gas and the oil will become immiscible because both phases are located at the side of the critical tie line. CO_2 does not offer significant benefits in this mechanism alone, but a combination of both mechanisms generates an enriched mixing zone with improved mobility characteristics that may benefit the displacement process (Lake, 1989, Mathiassen, 2003).

Minimum Miscibility Pressure

Two immiscible fluids may become miscible if the pressure is elevated. The degree of miscibility between an injected gas and a reservoir oil is commonly related to the minimum miscibility pressure, MMP. The MMP is the lowest pressure at which oil and gas phases through multiple-contact processes between the reservoir oil and the injected gas are miscible in all proportions (Lake, 1989, Zolotukhin and Ursin, 2000, Mathiassen, 2003). MMP depends on reservoir crude oil and injected solvent compositions and is determined by conducting slim tube tests. Accurate predictions of MMP is important when determining necessary conditions for near-miscible or miscible displacements. Miscible displacement processes has the ability to recover 15-20% additional OOIP, compared with only 5-10% during immiscible displacements (Lake, 1989).

Appendix III – Uncertainties

Calculating uncertainties

$y = f(x_1, x_2, x_3, \dots)$

y is a function of several variables x_1, x_2, x_3,…, with related uncertainties Sx_1, Sx_2, Sx_3,…

Mean

Independent variables *x, y, z*,… all have arithmetical mean values $\bar{x}, \bar{y}, \bar{z}$… that can be calculated by:

$$\bar{x} = \frac{x_1 + x_2 + x_3 + \cdots + x_N}{N} = \frac{1}{N}\sum_{i=1}^{N} x_i \qquad \textbf{A.7}$$

The uncertainty of the mean value can be calculated via the min-max theorem for $3 \le N \le 11$:

$$S_{\bar{x}} \approx \frac{W_N}{\sqrt{N}} = \frac{x_{max} - x_{min}}{\sqrt{N}} \qquad \textbf{A.8}$$

Addition and subtraction

For a value *R* calculated by addition or subtraction of uncorrelated variables *x*, *y*, *x*,… where each variable introduces an uncertainty S_x, S_y, S_z,… the uncertainty for *R* denoted S_R can be written as:

$$S_R = \sqrt{\left(\frac{\delta R}{\delta x} S_x\right)^2 + \left(\frac{\delta R}{\delta y} S_y\right)^2 + \left(\frac{\delta R}{\delta z} S_z\right)^2 + \cdots} \qquad \textbf{A.9}$$

Products

The uncertainty of value *R* given as a product of uncorrelated variables *x*, *y*, *z*,… can be written as:

$$\frac{S_R}{R} = \sqrt{\left(a\frac{S_x}{x}\right)^2 + \left(b\frac{S_y}{y}\right)^2 + \left(c\frac{S_z}{z}\right)^2 + \cdots} \qquad \textbf{A.10}$$

Instrumental Uncertainties

- ESI Pressure transducer (Max. pressure 250 bar): ± 0.1% of full scale
- Quizix Q5000 Series pump, injection rate: ± 2% ml/h
- Quizix QX-1500 pump, injection rate: ± 2% ml/h
- Instrument used to measure core sample weight: ± 0.01 g
- Graded cylinder deviation: ± 0.05 ml
- Caliper used to measure length and diameter: ± 0.01 cm

Sources of Error

The experimental work done in this thesis is associated with sources of error and related uncertainties that may affect the accuracy of measurements. Sources of significance are presented in this section.

Graded cylinder production reading: Liquid production was accumulated in 35 ml graded cylinders and the oil production was measured by reading the total liquid production and water production and calculating the difference. However, in some of the experiments, especially during the co-injection, the liquid production proved to be difficult to read because of oil clinging to the cylinder walls. Figure A.4 illustrates a situation where accurate liquid production reading might be difficult to obtain. This effect was reduced if given enough time for the liquid solution and the crude oil to separate and settle.

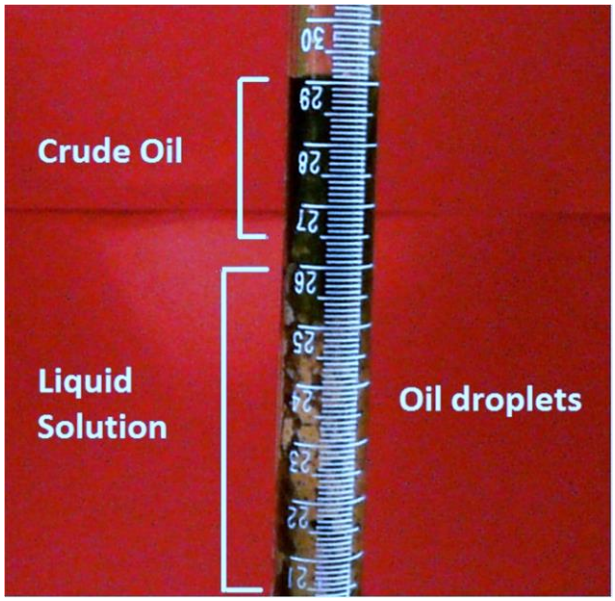

Figure A.4: Webcam picture of the graded cylinder accumulating the liquid production in CO2F3. The picture was taken upon reaching 2.8 PV injected during the co-injection. Small segments of oil was observed along the glass cylinder.

Pressure fluctuations: The pressure monitored showed fluctuations during the absolute permeability measurements. Observed pressure for each flow rate is noted and may cause inaccurate calculations.

Back Pressure Regulator: After concluding each experiment, the BPR was disassembled for cleaning and damage control. Varying amounts of crude oil and liquid solution was observed inside the BPR. However, the volume of the liquid inside the BPR did not constitute to a significant amount.

Pump cylinder pressure: Both pumps used in the experimental work did not always show pressure correlation with the observed tubing line pressure monitored with the ESI pressure transducers.

Dead volume: Dead volume in Swagelock 1/8" diameter tubing lines, valves and fittings was calculated to account for the additional volume of liquid produced during the waterfloods and the co-injections. Volumetric uncertainties may affect actual liquid production and consequently the oil recovery.

Timing: Because of the added volume of tubing lines between the core holder and the production cylinder, actual liquid produced from the stacked cores must be corrected in time. This is done to so that 0.0^{+} PV injected correlates with the first observed liquid production from the stacked cores.

Appendix IV – References

AL-SHURAIQI, H. S., MUGGERIDGE, A. H. & GRATTONI, C. A. 2003. Laboratory Investigations of First Contact Miscible WAG Displacement: The Effects of WAG Ratio and Flow Rate. *Society of Petroleum Engineers.* Kuala Lumpur, Malaysia.

ALLAN, J. & SUN, S. Q. 2003. Controls on Recovery Factor in Fractured Reservoirs: Lessons Learned from 100 Fractured Fields. *In:* ENGINEERS, S. O. P. (ed.) *SPE Annual Technical Conference and Exhibition, 5-8 October.* Denver, Colorado, U.S.: Society of Petroleum Engineers.

BASHIRI, A. & KASIRI, N. 2011. Properly Use Effect of Capillary Number on Residual Oil Saturation. *Nigeria Annual International Conference and Exhibition, 30 July - 3 August.* Abuja, Nigeria: Society of Petroleum Engineers.

CRAZE, R. C. 1950. Performance of Limestone Reservoirs. *SPE Journal Paper,* 2.

ENICK, R. M. & OLSEN, D. K. 2012. Mobility and Conformance Control for Carbon Dioxide Enhanced Oil Recovery (CO2-EOR) via Thickeners, Foams and Gels - A Detailed Literature Review of 40 Years of Research. *DOE/NETL-2012/1540*.

FARAJZADEH, R., ANDRIANOV, A. & ZITHA, P. L. J. 2010. Investigation of Immiscible and Miscible Foam for Enhancing Oil Recovery. Delft, The Netherlands: Delft University of Technology.

FARELAS, F., CHOI, Y. S. & NESIC, S. 2012. Effects of CO2 Phase Change, SO2 Content And Flow On the Corrosion of CO2 Transmission Pipeline Steel. *CORROSION 2012, 11-15 March.* Salt Lake City, Utah, United States: NACE International.

FERNØ, M. 2012. Enhanced Oil Recovery in Fractured Reservoirs. University of Bergen, Bergen, Norway: Department of Physics and Technology, University of Bergen

FERNØ, M. A., HAUGEN, Å. & GRAUE, A. 2012. Surfactant Prefloods for Integrated EOR in Fractured, Oil-Wet Carbonate Reservoirs. *SPE Journal Paper*.

GAUTEPLASS, J., CHAUDHARY, K., KOVSCEK, A. R. & FERNØ, M. A. 2014. Pore-level Foam Generation and Flow for Mobility Control in Fractured Systems *In:* ADLER, M., GRIESER, F., LI, J. B. & PRIEVE, D. (eds.) *Colloids and Surfaces A: Physicochemical and Engineering Aspects.*

GCCSI 2015. The Global Status of CCS Melbourne, Australia: Global CCS Institute, Australia.

GRAUE, A., VIKSUND, B. G., BALDWIN, B. A. & SPINLER, E. A. 1999. Large-Scale Two-Dimensional Imaging of Wettability Effects on Fluid Movement and Oil Recovery in Fractured Chalk. *SPE Journal Paper,* 4**,** 25-36.

HAMON, G. 2004. Another Look At Ekofisk Wettability. *the International Symposium of the Society of Core Analysts, 5-9 October 2004.* Abu Dhabi: Society of Core Analysts.

HANDY, L. L., AMAEFULE, J. O., ZIEGLER, V. M. & ERSHAGHI, I. 1982. Thermal Stability of Surfactants for Reservoir Application *SPE Journal Paper,* 22**,** 722 - 730.

HAUGEN, Å., FERNØ, M. A., GRAUE, A. & BERTIN, H. J. 2010. Experimental study of foam flow in fractured oil-wet limestone for enhanced oil recovery.

HAUGEN, Å., MANI, N., SVENNINGSEN, S., BRATTEKÅS, B., GRAUE, A., ERSLAND, G. & FERNØ, M. A. 2014. Miscible and Immiscible Foam Injection for Mobility Control and EOR in Fractured Oil-Wet Carbonate Rocks. *In:* BLUNT, M. J. (ed.) *Transport In Porous Media.* Springer.

HJARTNES, T. 2015. *An Experimental Study of Tertiary CO2 Injection Strategies in Fractured Limestone Rocks.* Masters, University of Bergen.

HOLM, L. W. 1986. Miscibility and Miscible Displacement. *Journal of Petroleum Technology*.

HOLM, L. W. & JOSENDAL, V. A. 1974. Mechanisms of Oil Displacement By Carbon Dioxide. *SPE Journal Paper,* 26.

IEA 2015. CO2 Emissions from fuel combustion. IEA.org: International Energy Agency.

IPCC 2014. Climate Change 2014. IPCC: Intergovernmental Panel on Climate Change (IPCC).

JIAN, M. G., CUI, L., BISWAL, L. & HIRASAKI, G. 2015. CO2 Foam Mobility Control and Adsorption with Nonionic Surfactant. RICE University.

KAVOUSI, A., TORABI, F., CHAN, C. W. & SHIRIF, E. 2014. Experimental measurement and parametric study of CO2 solubility and molecular diffusivity in heavy crude oil systems. Elsevier: Faculty of Engineering and Applied Science, University of Regina.

KOVSCEK, A. R. & RADKE, C. J. 1993. Fundamentals of Foam Transport in Porous Media.

LAKE, L. W. 1989. *Enhanced Oil Recovery,* Englewood Cliffs, New Jersey, Prentice Hall.

LAMBERT, M. R., MARINO, S. D., ANTHONY, T. L., CALVIN, M. W., GUTIERREZ, S. & SMITH, D. P. 1996. Implementing CO2 Floods: No More Delays! *Permian Basin Oil and Gas Recovery Conference, 27-29 March.* Midland, Texas, U.S. : Society of Petroleum Engineers.

LIEN, J. R., JAKOBSEN, M. & SKAUGE, A. 2007. Introduction to Petroleum- and Process Technology. University of Bergen: University of Bergen.

LUCIA, F. J. 2007. *Carbonate Reservoir Characterization - An Integrated Approach (Second Edition),* Springer-Verlag Berlin Heidelberg, Springer Berlin Heidelberg.

LUCIA, F. J., KERANS, C. & JR., J. W. J. 2003. Carbonate Reservoir Characterization. *SPE Journal Paper,* 55**,** 70-72.

MARTIN, D. F. & TABER, J. J. 1992. Carbon Dioxide Flooding. *SPE Journal Paper,* 44**,** 396-400.

MARZOUK, I., TAKEZAKI, H. & SUZUKI, M. 1998. New Classification of Carbonate Rocks for Reservoir Characterization. *Abu Dhabi International Petroleum Exhibition and Conference, 11-14 November.* Abu Dhabi, United Arab Emirates: Society of Petroleum Engineers (SPE).

MATHIASSEN, O. M. 2003. CO2 as Injection Gas for Enhanced Oil Recovery and Estimation of the Potential on the Norwegian Continental Shelf.

MELBY, T. A. 2014. *Optimizing CO2-injection by Compositional Simulation.* MSc, Norwegian University of Science and Technology.

MOORTGAT, J. B., FIROOZABADI, A., LI, Z. & ESPÓSITO, R. O. 2013. CO2 Injection in Vertical and Horizontal Cores: Measurements and Numerical Simulation. *Society of Petroleum Engineers,* 18**,** 331-344.

MUNGAN, N. 1981. Carbon Dioxide Flooding-Fundamentals. *PETSOC Journal Paper*.

NOLL, L. A. 1991. The Effect of Temperature, Salinity, and Alcohol on the Critical Micelle Concentration of Surfactants. *SPE Journal Paper*.

NPD. 2012. *Økt utvinning fra eksisterende felt* [Online]. https://www.norskoljeoggass.no/no/Faktasider/Okt-utvinning/. [Accessed 10.05 2016].

NPD. 2015. *Remaining Reserves Per Area as of 31.12.2015* [Online]. http://www.norskpetroleum.no/en/facts/remaining-reserves/. [Accessed].

OFE. 2013. *Enhanced Oil Recovery* [Online]. http://energy.gov/fe/science-innovation/oil-gas-research/enhanced-oil-recovery: U.S. Department of Energy. [Accessed 25.04 2016].

PICHA, M. S. 2007. Enhanced Oil Recovery By Hot CO2 Flooding. *SPE Middle East Oil and Gas Show and Conference, 11-14 March.* Manama, Bahrain: Society of Petroleum Engineers.

RANSOHOFF, T. C. & RADKE, C. J. 1988. Mechanisms of Foam Generation in Glass-Bead Packs. *SPE Journal Paper,* 3**,** 573 - 585.

ROGERS, J. D. & GRIGG, R. B. 2001. A Litterature Analysis of the WAG Injectivity Abnormalities in the CO2 Process. *Society of Petroleum Engineers,* 4**,** 375-386.

ROSSEN, W. R. 2003. A critical review of Roof snap-off as a mechanism of steadystate foam generation in homogeneous porous media. Austin, Texas: Department of Petroleum and Geosystems Engineering, The University of Texas in Austin.

SASAKI, K., SUGAI, Y., CHANMOLY, O. R. & KONO, H. 2013. CO2 Solubility Characteristics of Crude Oils related to Carbon Capture and Utilization (CCU). *NOVEL CARBON RESOURCE SCIENCES NEWSLETTER*.

SCHRAMM, L. L. & WASSMUTH, F. 1994. Foams: Basic Principles. *In:* SCHRAMM, L. L. (ed.) *Foams: Fundamentals and Applications in the Petroleum Industry.* American Chemical Society.

SIDIQ, H. H. & AMIN, R. 2010. Supercritical CO2/Methane Relative Permeability Investigation. *SPE International Conference on CO2 Capture, Storage, and Utilization, 10-12 November.* New Orleans, Louisiana, U.S.: Society of Petroleum Engineers.

SKAUGE, A. 2013. Pore Scale Physics and Network Modeling. University of Bergen, Bergen, Norway: Centre of Integrated Petroleum Researcs.

SLB 2014. *Eclipse: Industry Reference Reservoir Simulator (Training and Exercise Guide)*, NExT: A Schlumberger Company.

SLOAN, E. D. & KOH, C. A. 2008. *Clathrate Hydrates of Natural Gases, Third Edition,* Colorado School of Mines, CRC Press.

SORBIE, K. S. & DIJKE, M. I. J. V. 2005. Fundamentals of Three-Phase Fluid Flow in Porous Media of Heterogeneous Wettability. Heriott-Watt University, Edunburgh, Scotland UK: Institute of Petroleum Engineering.

SUNDSET, T. 2011. Latest Development in Carbon Capture and Sequestration. *20th World Petroleum Congress.* 4-8 December, Doha, Qatar: World Petroleum Council.

TANZIL, D., HIRASAKI, G. J. & MILLER, C. A. 2002. Conditions for Foam Generation in Homogeneous Porous Media. *SPE/DOE Improved Oil Recovery Symposium, 13-17 April.* Tulsa, Oklahoma: Society of Petroleum Engineers.

WALLACE, M. & KUUSKRAA, V. 2014. Near-Term Projections of CO2 Utilization for Enhanced Oil Recovery. U.S. Department of Energy / National Energy Technology Laboratory.

WARD, C. H. 2016. *NAPL Removal Surfactants, Foams and Microemulsions*, CRC Press.

WEC 2013. World Energy Scenarios - Composing energy futures to 2050. WorldEnergy.org: WEC: World Energy Council.

ZIEGLER, V. M. & HANDY, L. L. 1981. Effect of Temperature on Surfactant Adsorption in Porous Media. *SPE Journal Paper,* 21.

ZOLOTUKHIN, A. B. & URSIN, J.-R. 2000. *Introduction to Petroleum Reservoir Engineering*, Norwegian Academic Press.

Appendix V – Simulation Data File

BL1_SIM.DATA

```
RUNSPEC
NOECHO
TITLE
EXP-1 : E 13-16-14-15
WATER
OIL
METRIC
DIMENS
 1 1 400 /
EQLDIMS
 4 /
TABDIMS
 2 1 2* 4 /
WELLDIMS
 5 5 5 5 /
START
 11 FEB 2016 09:20:00 /
UNIFIN
UNIFOUT
ENDSCALE
/
OPTIONS
 234*  1 /
MESSAGES
 6* 4*10000000 /

---------------------------------------------------------

GRID
INIT
GRIDFILE
 0 1 /
INCLUDE
 'INCLUDE/GRID.INC' /
PORO
 100*0.262 100*0.270 100*0.261 100*0.253 /
PERMZ
 100*64.5 100*62.3 100*53.5 100*47.4 /
COPY
 PERMZ PERMX /
 PERMZ PERMY /
/
MINPV
 0.000000001  /
RPTGRID
 ALLNNC DX DY DZ TOPS PORO PORV /

 ---------------------------------------------------------

EDIT

---------------------------------------------------------

PROPS
INCLUDE
 'INCLUDE/PROPS.INC' /
---------------------------------------------------------

REGIONS
EQLNUM
 100*1 100*2 100*3 100*4 /
SATNUM
 98*1 2*2 98*1 2*2 98*1 2*2 98*1 2*2 /
FIPNUM
 100*1 100*2 100*3 100*4 /
PVTNUM
 400*1 /

---------------------------------------------------------

SOLUTION
PRESSURE
 100*84.42 100*84.42 100*84.42 100*84.42 /
SWAT
 100*0.290 100*0.290 100*0.290 100*0.290 /
RPTRST
 BASIC=2 /

---------------------------------------------------------

SUMMARY
INCLUDE
 'INCLUDE/SUMMARY.INC' /
RPTONLY

---------------------------------------------------------

SCHEDULE
TUNING
0.0006 0.0013 0.0003 0.0003 /
/
4* 500 /
RPTSCHED
 WELLS /
RPTRST
 BASIC=2 /
OPTIONS
 234*  1 /
WELSPECS
 WINJ 'CORE' 1 1 1* WATER /
 PROD 'CORE' 1 1 1* OIL /
/
COMPDAT
--name I J   K1  K2 STATUS   DIAM     DIREC
 WINJ 1 1   1   1 OPEN 2* 0.00439 3* Z /
 PROD 1 1 400 400 OPEN 2* 0.00439 3* Z /
/
GRUPTREE
 'CORE' FIELD /
/
INCLUDE
 'INCLUDE/SCHEDULE.INC' /
END
```

PROPS.INC

```
ROCK
     80.0000  4.3147E-005 /
PVTW
        80      1.0078  4.1088E-005     0.49623          0 /
RSCONSTT
      20.106         50 /

PVDO
         50       1.079       3.0191
       52.632      1.0784       3.0291
       55.263      1.0778       3.0397
       57.895      1.0773       3.0509
       60.526      1.0769       3.0627
       63.158      1.0765       3.0751
       65.789      1.0761        3.088
       68.421      1.0757       3.1015
       71.053      1.0754       3.1155
       73.684      1.0751       3.1301
       76.316      1.0748       3.1452
       78.947      1.0746       3.1607
       81.579      1.0743       3.1768
       84.211      1.0741       3.1933
       86.842      1.0739       3.2103
       89.474      1.0737       3.2278
       92.105      1.0735       3.2457
       94.737      1.0733       3.2641
       97.368      1.0731       3.2829
        100       1.073       3.3022
 /

DENSITY
       875.3      1020.3      0.81172 /

SWOF
       0.29          0          1          0
       0.30       0.004       0.85          0
       0.40       0.04       0.40          0
       0.53       0.10       0.20          0
       0.58       0.13       0.15          0
       0.64       0.17       0.10          0
       0.69       0.21       0.06          0
       0.71       0.23      0.045          0
       0.76       0.29       0.02          0
       0.81       0.39      0.010          0
       0.87       0.60       0.00          0
       1.00          1          0          0
 /
       0.29          0          1          0
       0.30       0.004       0.85          0
       0.40       0.04       0.40          0
       0.53       0.10       0.20          0
       0.58       0.13       0.15          0
       0.64       0.17       0.10          0
       0.69       0.21       0.06          0
       0.71       0.23      0.045          0
       0.76       0.29       0.02          0
       0.81       0.39      0.010          0
       0.87       0.60       0.00          0
       1.00          1          0          0
 /
```

SUMMARY.INC

```
TIMESTEP

-- requested output simulation data

WBP
/
WBHP
/
WBHPH
/

WPI
/

WVIR
/
WVPR
/

WWIR
/
WOPR
/
WWPR
/
WWCT
/

WWIT
/
WOPT
/
WWPT
/

WWIRH
/
WOPRH
/
WWPRH
/
WWCTH
/

WWITH
/
WOPTH
/
WWPTH
/
WGPR
/
WGIR
/
```

SCHEDULE.INC

```
-- SCHEDULE EXPERIMENT 5 WATERFLOOD

WCONHIST
  PROD OPEN BHP 0.00024000 0.00000000 0 1* 1* 1*
82.7000 /
/
WCONINJH
  WINJ WATER OPEN 0.00024000 84.1000 /
/
DATES
  11 FEB 2016 09:21:00 /
/
WCONHIST
  PROD OPEN BHP 0.00024000 0.00000000 0 1* 1* 1*
82.4000 /
/
WCONINJH
  WINJ WATER OPEN 0.00024000 83.7000 /
/
DATES
  11 FEB 2016 09:36:00 /
/
WCONHIST
  PROD OPEN BHP 0.00024000 0.00000000 0 1* 1* 1*
82.7000 /
/
WCONINJH
  WINJ WATER OPEN 0.00024000 84.0000 /
/
DATES
  11 FEB 2016 09:51:00 /
/
WCONHIST
  PROD OPEN BHP 0.00024000 0.00000000 0 1* 1* 1*
82.8000 /
/
WCONINJH
  WINJ WATER OPEN 0.00024000 84.1000 /
/
DATES
  11 FEB 2016 10:10:00 /
/
WCONHIST
  PROD OPEN BHP 0.00024000 0.00000000 0 1* 1* 1*
82.4000 /
/
WCONINJH
  WINJ WATER OPEN 0.00024000 83.7000 /
/
DATES
  11 FEB 2016 10:30:00 /
/
WCONHIST
  PROD OPEN BHP 0.00024000 0.00000000 0 1* 1* 1*
82.5000 /
/
WCONINJH
  WINJ WATER OPEN 0.00024000 83.7000 /
/
DATES
  11 FEB 2016 10:50:00 /
/
WCONHIST
  PROD OPEN BHP 0.00024000 0.00000000 0 1* 1* 1*
82.5000 /
/
WCONINJH
  WINJ WATER OPEN 0.00024000 83.7000 /
/
DATES
  11 FEB 2016 11:09:00 /
/
WCONHIST
  PROD OPEN BHP 0.00024000 0.00000000 0 1* 1* 1*
82.5000 /
/
WCONINJH
  WINJ WATER OPEN 0.00024000 83.7000 /
/
DATES
  11 FEB 2016 11:25:00 /
/
WCONHIST
  PROD OPEN BHP 0.00024000 0.00000000 0 1* 1* 1*
82.4000 /
/
WCONINJH
  WINJ WATER OPEN 0.00024000 83.7000 /
/
DATES
  11 FEB 2016 11:45:00 /
/
WCONHIST
  PROD OPEN BHP 0.00024000 0.00000000 0 1* 1* 1*
82.6000 /
/
WCONINJH
  WINJ WATER OPEN 0.00024000 84.0000 /
/
DATES
  11 FEB 2016 12:00:00 /
/
WCONHIST
  PROD OPEN BHP 0.00024000 0.00000000 0 1* 1* 1*
82.5000 /
/
WCONINJH
  WINJ WATER OPEN 0.00024000 83.9000 /
/
DATES
  11 FEB 2016 12:20:00 /
/
WCONHIST
  PROD OPEN BHP 0.00024000 0.00000000 0 1* 1* 1*
82.6000 /
/
WCONINJH
  WINJ WATER OPEN 0.00024000 83.9000 /
/
DATES
  11 FEB 2016 12:36:00 /
/
WCONHIST
```

```
 PROD OPEN BHP 0.00023000 0.00001000 0 1* 1* 1*
82.5000 /
/
WCONINJH
 WINJ WATER OPEN 0.00024000 83.9000 /
/
DATES
 11 FEB 2016 12:51:00 /
/
WCONHIST
 PROD OPEN BHP 0.00017000 0.00007000 0 1* 1* 1*
82.5000 /
/
WCONINJH
 WINJ WATER OPEN 0.00024000 83.9000 /
/
DATES
 11 FEB 2016 13:03:00 /
/
WCONHIST
 PROD OPEN BHP 0.00008000 0.00016000 0 1* 1* 1*
82.5000 /
/
WCONINJH
 WINJ WATER OPEN 0.00024000 83.9000 /
/
DATES
 11 FEB 2016 13:18:00 /
/
WCONHIST
 PROD OPEN BHP 0.00006000 0.00018000 0 1* 1* 1*
82.4000 /
/
WCONINJH
 WINJ WATER OPEN 0.00024000 83.5000 /
/
DATES
 11 FEB 2016 13:33:00 /
/
WCONHIST
 PROD OPEN BHP 0.00006000 0.00018000 0 1* 1* 1*
82.5000 /
/
WCONINJH
 WINJ WATER OPEN 0.00024000 83.5000 /
/
DATES
 11 FEB 2016 13:57:00 /
/
WCONHIST
 PROD OPEN BHP 0.00005000 0.00019000 0 1* 1* 1*
83.0000 /
/
WCONINJH
 WINJ WATER OPEN 0.00024000 84.1000 /
/
DATES
 11 FEB 2016 14:13:00 /
/
WCONHIST
 PROD OPEN BHP 0.00006000 0.00018000 0 1* 1* 1*
82.3000 /
/
WCONINJH
 WINJ WATER OPEN 0.00024000 83.4000 /
/
DATES
 11 FEB 2016 14:27:00 /
/
WCONHIST
 PROD OPEN BHP 0.00005000 0.00019000 0 1* 1* 1*
82.8000 /
/
WCONINJH
 WINJ WATER OPEN 0.00024000 83.9000 /
/
DATES
 11 FEB 2016 14:40:00 /
/
WCONHIST
 PROD OPEN BHP 0.00004000 0.00020000 0 1* 1* 1*
81.6000 /
/
WCONINJH
 WINJ WATER OPEN 0.00024000 82.8000 /
/
DATES
 11 FEB 2016 14:52:00 /
/
WCONHIST
 PROD OPEN BHP 0.00005000 0.00019000 0 1* 1* 1*
83.0000 /
/
WCONINJH
 WINJ WATER OPEN 0.00024000 84.0000 /
/
DATES
 11 FEB 2016 15:15:00 /
/
WCONHIST
 PROD OPEN BHP 0.00005000 0.00019000 0 1* 1* 1*
82.7000 /
/
WCONINJH
 WINJ WATER OPEN 0.00024000 83.8000 /
/
DATES
 11 FEB 2016 15:35:00 /
/
WCONHIST
 PROD OPEN BHP 0.00002000 0.00022000 0 1* 1* 1*
81.6000 /
/
WCONINJH
 WINJ WATER OPEN 0.00024000 82.6000 /
/
DATES
 11 FEB 2016 15:50:00 /
/
WCONHIST
 PROD OPEN BHP 0.00002000 0.00022000 0 1* 1* 1*
82.5000 /
/
WCONINJH
 WINJ WATER OPEN 0.00024000 83.6000 /
/
```

```
DATES
 11 FEB 2016 16:10:00 /
/
WCONHIST
 PROD OPEN BHP 0.00002000 0.00022000 0 1* 1* 1*
81.7000 /
/
WCONINJH
 WINJ WATER OPEN 0.00024000 82.7000 /
/
DATES
 11 FEB 2016 16:23:00 /
/
WCONHIST
 PROD OPEN BHP 0.00001000 0.00023000 0 1* 1* 1*
82.7000 /
/
WCONINJH
 WINJ WATER OPEN 0.00024000 83.8000 /
/
DATES
 11 FEB 2016 16:50:00 /
/
WCONHIST
 PROD OPEN BHP 0.00003000 0.00021000 0 1* 1* 1*
82.9000 /
/
WCONINJH
 WINJ WATER OPEN 0.00024000 83.8000 /
/
DATES
 11 FEB 2016 17:15:00 /
/
WCONHIST
 PROD OPEN BHP 0.00005000 0.00019000 0 1* 1* 1*
82.3000 /
/
WCONINJH
 WINJ WATER OPEN 0.00024000 83.1000 /
/
DATES
 11 FEB 2016 17:40:00 /
/
WCONHIST
 PROD OPEN BHP 0.00003000 0.00021000 0 1* 1* 1*
82.6000 /
/
WCONINJH
 WINJ WATER OPEN 0.00024000 83.4000 /
/
DATES
 11 FEB 2016 18:03:00 /
/
WCONHIST
 PROD OPEN BHP 0.00002000 0.00022000 0 1* 1* 1*
82.6000 /
/
WCONINJH
 WINJ WATER OPEN 0.00024000 83.4000 /
/
DATES
 11 FEB 2016 18:20:00 /
/
WCONHIST
 PROD OPEN BHP 0.00002000 0.00022000 0 1* 1* 1*
82.6000 /
/
WCONINJH
 WINJ WATER OPEN 0.00024000 83.4000 /
/
DATES
 11 FEB 2016 18:40:00 /
/
WCONHIST
 PROD OPEN BHP 0.00004000 0.00020000 0 1* 1* 1*
82.5000 /
/
WCONINJH
 WINJ WATER OPEN 0.00024000 83.5000 /
/
DATES
 11 FEB 2016 19:00:00 /
/
WCONHIST
 PROD OPEN BHP 0.00004000 0.00020000 0 1* 1* 1*
82.5000 /
/
WCONINJH
 WINJ WATER OPEN 0.00024000 83.1000 /
/
DATES
 11 FEB 2016 19:15:00 /
/
WCONHIST
 PROD OPEN BHP 0.00000000 0.00024000 0 1* 1* 1*
82.7000 /
/
WCONINJH
 WINJ WATER OPEN 0.00024000 82.8000 /
/
DATES
 11 FEB 2016 19:35:00 /
/
WCONHIST
 PROD OPEN BHP 0.00001000 0.00023000 0 1* 1* 1*
82.3000 /
/
WCONINJH
 WINJ WATER OPEN 0.00024000 83.0000 /
/
DATES
 11 FEB 2016 20:05:00 /
/
WCONHIST
 PROD OPEN BHP 0.00000000 0.00024000 0 1* 1* 1*
82.8000 /
/
WCONINJH
 WINJ WATER OPEN 0.00024000 83.9000 /
/
DATES
 11 FEB 2016 20:34:00 /
/
```